Chemosphere 268 (2021) 129328

Contents lists available at ScienceDirect

Chemosphere

journal homepage: www.elsevier.com/locate/chemosphere

Polydopamine functionalized graphene sheets decorated with magnetic metal oxide nanoparticles as efficient nanozyme for the detection and degradation of harmful triazine pesticides

Purna K. Boruah [a, b], Gitashree Darabdhara [a, b], Manash R. Das [a, b, *]

[a] Advanced Materials Group, Materials Sciences and Technology Division, CSIR-North East Institute of Science and Technology, Jorhat, 785006, Assam, India
[b] Academy of Scientific and Innovative Research, Ghaziabad, 201002, India

HIGHLIGHTS

- In situ formation of polydopamine functionalization graphene sheets (DG).
- Well distributed Fe_3O_4 NPs deposited on DG sheets by in situ approach.
- Fe_3O_4/DG established as a nanozyme towards triazine pesticide detection.
- Highly selective detection activity of Fe_3O_4/DG nanozyme towards simazine pesticide.
- Fe_3O_4/DG also utilized as a sunlight-assisted photocatalyst for simazine degradation.

GRAPHICAL ABSTRACT

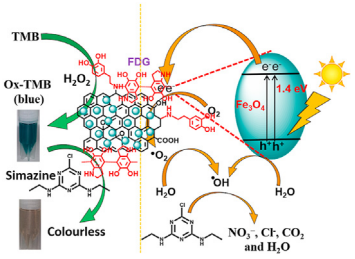

ARTICLE INFO

Article history:
Received 30 April 2020
Received in revised form
7 December 2020
Accepted 13 December 2020
Available online 15 December 2020

Handling Editor: Grzegorz Lisak

Keywords:
Polydopamine functionalized graphene
Nanozyme
Detection
Photocatalyst
Degradation

ABSTRACT

A facile and an eco-friendly reduction and functionalization of reduced graphene oxide (rGO) sheets is carried out using dopamine and decorated with magnetic Fe_3O_4 nanoparticles with an average size of 12 nm by a simple co-precipitation method which is established as an artificial nanozyme. Here, functionalization of graphene using dopamine has introduced several advantages and insights into this study. The Fe_3O_4 nanoparticles decorated functionalized rGO sheets (FDGs) nanozymes are characterized by X-ray diffraction (XRD), X-ray photoelectron spectroscopy (XPS), high-resolution transmission electron microscopy (HRTEM), Raman spectroscopy, atomic force microscopy (AFM), thermogravimetric (TGA) and vibrating sample magnetometer (VSM) analysis. FDGs nanozymes exhibits dual characteristics towards detection and degradation of harmful simazine pesticide. The hydrogen bonding interactions between pesticide molecules and 3,3′,5,5′-tetramethylbenzidine (TMB) causes inhibition of the catalytic activity of the FDGs towards oxidation of TMB molecule. Based on that, the presence of simazine pesticide in an aqueous medium can be easily determined and a certain value (2.24 μM) of detection limit was achieved. The photocatalytic degradation of simazine is also executed and excellent photocatalytic activity was observed under irradiation of direct natural sunlight. The FDGs nanozyme is also reusable up to several times with insignificant loss in its catalytic activity towards simazine degradation.

1. Introduction

With the increasing world population, pesticide use in agricultural fields is escalating at an alarming rate (Muenchen et al., 2016).

* Corresponding author. Terials Sciences & Technology Division, CSIR−North East Institute of Science and Technology, Jorhat, 785006, Assam, India..
E-mail addresses: mnshrdas@yahoo.com, mrdas@neist.res.in (M.R. Das).

https://doi.org/10.1016/j.chemosphere.2020.129328
0045-6535/

The wider applications of pesticides have turned fatal to human health as well as the environment due to their high toxicity (Devipriya and Yesodharan, 2005). Amongst the pesticides used in the agricultural fields, simazine, a triazine class of pesticide is widely used (Bonansea et al., 2013; Sekhon, 2014). Traces of simazine in μg L^{-1} in water bodies have the potential causing kidney congestion, low blood pressure, heart, adrenal gland and lung as confirmed by the United States Environmental Protection Agency (USEPA) (Agdi et al., 2000; Segura et al., 2007; Clemente et al., 2014). Triazine pesticide can bind receptor hormones such as endogen and estrogen which interfere with the central nervous system and development of the brain and this effect is called the endocrine-disrupting effect (Mnif et al., 2011). Therefore, constant monitoring and mitigating of pesticides in the surface water is highly necessary for the survival of human and animal life.

Conventional methods like high-performance liquid chromatography (HPLC), gas chromatography, and mass spectrometry, are generally used for pesticide detection which are however expensive as well as time consuming and requires skillful personnel (Shim et al., 2006; Graziano et al., 2006; Kaur et al., 2007; Huang et al., 2006). Therefore, the development of a facile method is highly desirable for pesticide detection. The colorimetric detection technique is one of the most efficient and simple techniques for detecting different organic and inorganic pollutants (Huang et al., 2019). In this method, the detection of the molecules takes place based on the color changes of the reaction medium (Huang et al., 2019).

Nanomaterials that behave like natural enzymes are termed as nanozymes and they are generally mass-produced, low cost and stable as compared to the natural enzymes (Wu et al., 2019). However, several drawbacks like high purification and operation cost, denaturation problem and high sensitivity towards environmental changes are inevitably associated with natural enzymes (Hosseini et al., 2017). Thus, researchers have developed several nanozymes to replace natural enzymes since the first utilization of Fe_3O_4 nanoparticles (NPs) as enzyme mimics in 2007 (Wu et al., 2019; Gao et al., 2007). However, the detection of pesticides using artificial nanozyme is scanty in literature. Li et al. utilized the Au NPs for the Malathion pesticide detection (Li et al., 2019). However, due to cost-related issues, the use of enzyme mimics was restricted for water contaminant detection (Li et al., 2019).

The removal of pesticides from the aqueous medium after their detection is another essential criterion in producing pesticide free water. Thus, several techniques like electrochemical degradation, membrane filtration, nanofiltration, adsorption, oxidation, photocatalytic degradation, etc. were adopted for the removal of pesticides (Srivastava et al., 2009). The heterogeneous photocatalytic degradation process is considered as the most efficient technologies for removing water contaminants. In this technique, direct decomposition of organic pollutants to nontoxic molecules and ions takes place without generating any toxic by-products (Bai et al., 2013; Wu et al., 2013; Sheng et al., 2013; Chen et al., 2013).

Graphene, the single atomic layer allotrope of graphite possesses high intrinsic surface area, large electron mobility, high electrical charge carrier, high optical transparency, mechanical flexibility and capability of functionalization (Kamat, 2010; Lomeda et al., 2008; Wang et al., 2011). Graphene supported semiconductors demonstrate enhanced photocatalytic activities and as such, they have enhanced charge separation capabilities via capturing conduction band (CB) electron to its surface and thus displays anti-photo-corrosion activity for various photocatalytic applications (Weng et al., 2019). Palaniappan et al. reported graphene for improving the corrosion resistance of the other materials in acid and salt environments (Palaniappan et al., 2019). Again, the functionalized rGO has outstanding electrical properties and it also ensures enhanced interaction between targeted water contaminants and composite materials by π-π interactions (Avinash et al., 2010; Lin et al., 2012). In the Fe_3O_4 nanoparticles decorated functionalized rGO sheets (FDGs) nanozymes reported in this publication, the functionalization of graphene using dopamine has introduced several advantages and insights into this study. Dopamine an abundant catecholamine is of particular interest in functionalizing graphene as it has a strong interaction with graphene and metal oxides (Kaminska et al., 2012). Dopamine is a multifunctional biopolymer and surface-adherent, which is self-polymerized during functionalization and acts as a reducing agent for GO reduction (Lee et al., 2007; Xu et al., 2010a). Yang and his co-workers reported that each graphene sheets sandwiched between two polydopamine due to functionalization prevents the restacking and agglomeration of graphene sheets as well as increases its surface area (Yang et al., 2012). However, practical implementation of the above-mentioned composites for water contaminant removal is limited due to the problem of their separation, recovery and reusability after photocatalytic reactions. Therefore, the development of nanocatalysts with magnetic properties is one of the most thrilling and growing topics of research (Wang and Astruc, 2014; Polshettiwar et al., 2011; Laurent et al., 2008; Metin et al., 2014). Amongst the magnetic nanomaterials, Fe_3O_4 (magnetite) is one of the highly abundant challenging materials with low toxicity, low cost, eco-friendly and high adsorptive properties (Akbarzadeh et al., 2012; Ghandoor et al., 2012). Fe_3O_4 is a low band gap (1.4 eV) visible light-responsive semiconductor and thus electron-hole pair recombination can easily occur in bare Fe_3O_4 during the photocatalytic degradation. Also, bare Fe_3O_4 NPs easily undergo agglomeration in an aqueous medium (Dong et al., 2009; Lee et al., 2011). Thus, the introduction of functionalized graphene not only reduces their agglomeration but also inhibits the electron-hole pair recombination (Chen et al., 2011; Varhese et al., 2009; R Rao et al., 2009).

With the above-mentioned views, we herein report the synthesis of Fe_3O_4/polydopamine functionalized graphene (FDGs) nanocomposites, which is further established as a nanozyme for the detection and degradation of harmful pesticide, simazine. The structure of simazine pesticide is shown in Fig. S1. To the best of our knowledge, until now no report on the colorimetric detection and photocatalytic degradation of simazine has been published using FDGs nanozymes. The LOD value of 2.24 μM for detection of simazine and 99% of simazine degradation were achieved using FDGs nanozymes.

2. Experimental

2.1. Materials

Graphite powder (<20 μm, Sigma-Aldrich, Germany), HCl (AR grade, Qualigens, India), H_2O_2 (30% w/v, Qualigens, India), $KMnO_4$ (>99%, NICE-Chemical, India), sulfuric acid (AR grade, Qualigens, India), NaOH (99%, Qualigens, India), NH_3 (25% E-Merck, Germany), dopamine hydrochloride (Sigma Aldrich, USA), Iron (III) chloride tetrahydrate (Merck, Germany), $FeCl_2{\cdot}4H2O$ (Across organics, Belgium) and 3,3′,5,5′-tetramethylbenzidine (TMB, Sigma Aldrich, USA), ethanol (Merck, Germany), simazine (Sigma-Aldrich, Germany) prometryn (Sigma-Aldrich, Germany), ametryn (Sigma-Aldrich, Germany), simeton (Sigma-Aldrich, Germany), atrazine (Sigma-Aldrich, Germany), Malathion Pestanal (Sigma-Aldrich, USA), Chloropyrifos Pestanal (Sigma-Aldrich, USA), Dibrom Pestanal (Sigma-Aldrich, USA) and Methidathion Pestanal (Sigma-Aldrich, USA) were used as received and without any further purification.

2.2. Synthesis of graphene oxide (GO) and polydopamine functionalized graphene (DG)

GO was prepared using a modified Hummers and Offermann method, which is reported in our previous publication (Das et al., 2011). In a typical synthesis of DG, 12 mL of GO solution (0.53 mg/mL) was taken in a round bottom flask (RB) and a tris buffer solution (30 mL, pH 8.5) was added to it under magnetic stirring. Then 15 mg of dopamine hydrochloride was added to the above suspension and heated at 60 °C for 24 h to produce the desired DG. Then the product was separated by centrifugation and washed with deionized (DI) water to remove the excess monomer.

2.3. Synthesis of Fe_3O_4/DG nanozyme

10 mL (1 mg L^{-1}) well dispersed DG sheets was taken in an RB and then 25% dilute NH_3 solution was added dropwise in this RB to attain the pH around 11. The reaction mixture was then transferred to an RB and magnetically stirred at room temperature. To synthesize Fe_3O_4/DG in the ratio (w/w) 20:1, 200 mg of $FeCl_2 \cdot 4H_2O$ and $FeCl_3.6H_2O$ (1:1 ratio) was added very slowly. After 4 h stirring, a black suspension was appeared, indicating the ferric and ferrous salts were oxidized and anchored at the surface of DG nanosheets by chemical interactions leading to the formation of Fe_3O_4/DG nanozyme. The Fe_3O_4/DG nanozyme was magnetically separated and washed with DI water. The obtained residue was dried in a hot air oven. Similarly, the Fe_3O_4/DG nanozyme of 15:1 and 10:1 ratio was synthesized by changing the initial amounts of $FeCl_2 \cdot 4H_2O$ and $FeCl_3.6H_2O$ salts. The synthesized polydopamine functionalized nanozymes in the ratio of 10:1, 15:1 and 20:1 of $FeCl_2 \cdot 4H_2O$ and $FeCl_3.6H_2O$ salts and GO were designated as FGD-10, FGD-15 and FGD-20, respectively. A schematic representation showing the formation of DG sheets and FDGs nanozyme are provided in Scheme 1. The functionalization and reduction of GO was achieved simultaneously via the oxidative polymerization of dopamine at weak alkaline condition (pH 8.5). Two electrons and protons were released during the polymerization of dopamine and they can attack carbon atoms those attached to the oxygen-containing functional group in the GO (Li et al., 2016). Thus, the reduced GO was attained by cleavage of hydroxyl group and restoration of the conjugated structure of graphene (Xu et al., 2010b; Cheng et al., 2013). As a result, GO was coated with polydopamine, which provides phenolic hydroxyl and amide groups (Li et al., 2016).

2.4. Characterization techniques

The characterization techniques details are provided in the Electronic Supplementary Information (ESI).

2.5. Peroxidase like catalytic activity of the FDG nanozyme

The oxidation of TMB to ox-TMB reaction has been carried out using H_2O_2 to investigate the peroxidase-like activity of the FDGs nanozyme. For the typical experiment, 9 mg L^{-1} FDGs nanozyme, 0.5 mM TMB solution and 50 μL H_2O_2 (30%) were added in 2.5 mL sodium acetate buffer solution (pH 4). The reaction mixture was

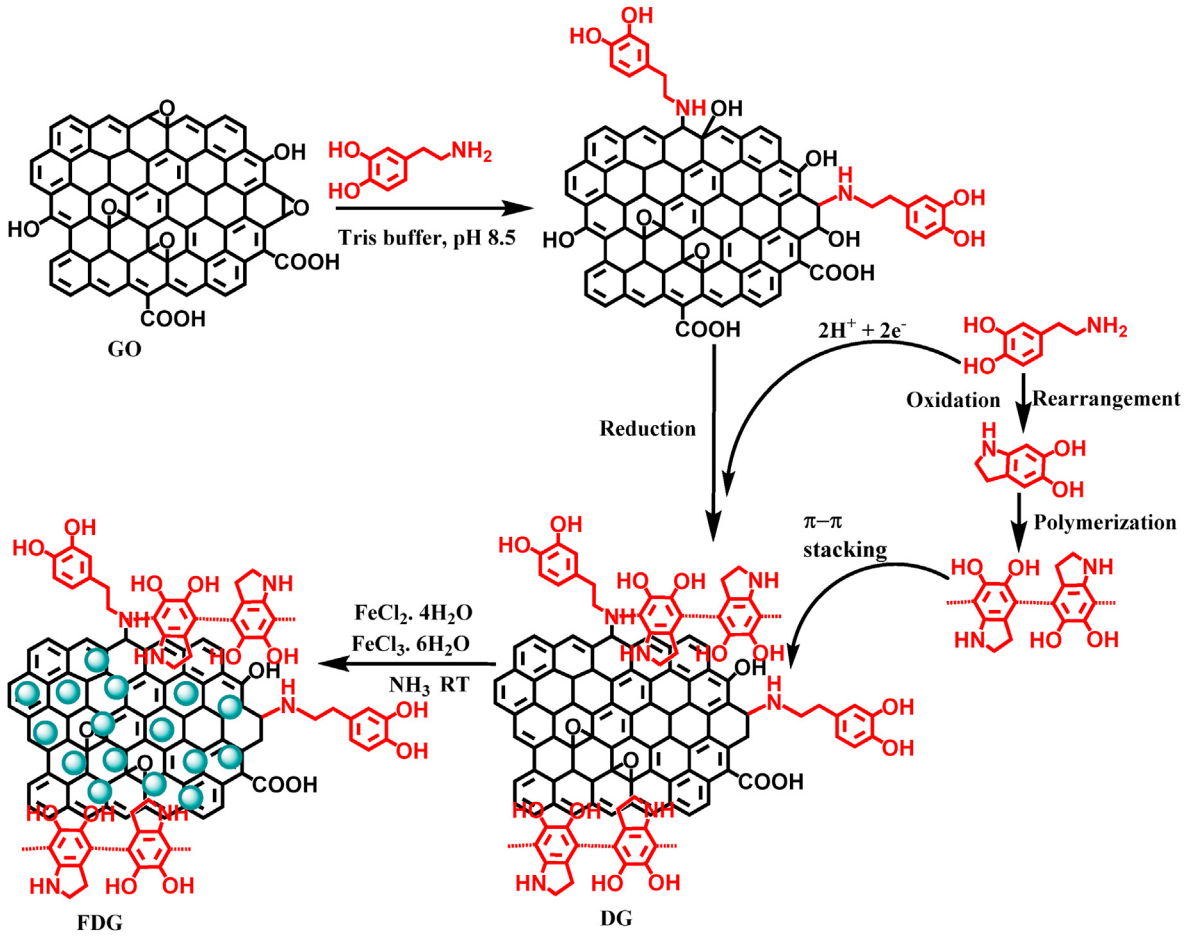

Scheme 1. Preparation of DG sheets and FDG nanozyme.

incubated at 30 °C for 30 min followed by monitoring the oxidation of TMB using a UV−visible spectrophotometer at a fixed wavelength (652 nm). The effect of varying H_2O_2 and TMB concentration was studied to investigate the enzyme kinetics. Michaelis-Menten constant (K_m) was obtained from the Lineweaver-Burk double reciprocal plot to predict the affinity of the enzyme regarding the substrate, which is optimized from the following equation.

$$\frac{1}{v} = \left(\frac{Km}{V\,max}\right)\left(\frac{1}{[S]}\right) + \left(\frac{1}{V\,max}\right) \quad (1)$$

where v represents the initial reaction rate, V_{max} is the maximal rate of the reaction and [S] determined the substrate concentration.

2.6. Generation of hydroxyl radicals during the TMB oxidation

The hydroxyl radicals (•OH) generated during the TMB oxidation reaction was studied using terephthalic acid (TA) as a probe molecule. Typically, TMB solution (0.5 mM), 50 μL (30%) H_2O_2 solution and 9 mg L^{-1} of FDGs nanozyme were added in 0.2 M sodium acetate buffer solution (2.5 mL, pH 4) along with TA (0.02 mM) and NaOH (0.02 mM). Then the above suspension was incubated for 30 min at 25 °C followed by monitoring TMB oxidation using a UV−visible spectrophotometer at 652 nm. The reaction mixtures were analysed by fluorescence spectrophotometer.

2.7. Colorimetric detection of the pesticides using FDG nanozyme

The simazine detection experiment was carried out in an aqueous medium by taking a different concentration of freshly prepared simazine (0.01−90 μM) with 0.5 mM TMB solution in 0.2 M sodium acetate buffer solution (2.5 mL, pH 5). After that, 50 μL H_2O_2 solution and 9 mg L^{-1} catalysts were added and the buffer solution was added to adjust the volume of 5 mL. The final reaction mixture was incubated for 30 min at 25 °C. The changes in the intensities at a wavelength of 652 nm due to ox-TMB (blue color) were studied by changing the simazine concentration.

2.8. Selectivity of FDG-20 nanozyme towards triazine pesticides detection

The selectivity of FDG-20 nanozyme towards simazine detection was investigated in the existence of different triazine pesticides such as ametryn, prometryn, simetone and atrazine and of different wastewater existing interfering ions like Ag^+, Cd^+, Pb^{2+} and Hg^{2+}. Also, the selectivity studies for simazine detection were carried out in presence of four different commonly used organophosphorus pesticides such as Malathion, Chloropyrifos, Dibrom and Methidathion followed by same experimental conditions of the simazine detection experimental procedure. However, the concentration of interfering ions and molecules (250 μM) was taken 5 times higher than the concentration of simazine and other triazine pesticides (50 μM).

2.9. Detection of simazine in the spiked environmental samples

The water samples from different sources such as a river, tube well and pond water samples were collected and spiked with 30, 40 and 50 μM of simazine to examine the practical applicability of FDGs nanozyme towards the detection of simazine. The water samples were collected from Brahmaputra (river water), CSIR-NEIST (tube well) and Mallow Pathar (pond water), Jorhat, India. Before spiking, the water samples were filtered by a 0.22 μm membrane filter. The simazine detection experiments were carried out in spiked water samples followed by colorimetric detection procedure as discussed in the section of pesticide detection test.

2.10. Photocatalytic degradation of pesticides using FDG nanozyme

The photocatalytic experiments for simazine degradation were mostly performed under sunlight irradiation. Moreover, the comparative photocatalytic degradation of simazine was performed under irradiation of UV light (125 W Neon lamp, wavelength: 254 nm) and visible light (400 W, visible lamp). The experiments under sunlight irradiated were executed on bright sunny days from 10 AM to 2 PM during March to July in the Jorhat City, India. The sunlight intensity was obtained using the solar power meter (KM SPM 11) and the average intensity during this time was 850 ± 20 W/m^2 30 mL of the reaction mixtures containing 0.3 mM simazine, and 0.3 g L^{-1} photocatalysts (FDGs) was stirred in dark to ensure the adsorption or desorption maximum. After that, the reaction mixture was irradiated in presence of sunlight and 2 mL of each reaction mixture was collected during this irradiation time at different intervals. The FDGs nanozyme were magnetically separated and the residual concentration of each supernatant was monitored using a UV−visible spectrophotometer. The degradation of pesticide was analysed by comparing with the calibration curve and the amount of degradation was calculated using the following equation.

$$\text{Degradation efficiency } (\%) = [1 - C_t / C_o] \times 100 \quad (2)$$

Where, C_o is the initial and C_t is the residual concentration of simazine at time t, respectively.

2.11. Reusability studies of the photocatalyst

After photocatalytic degradation of simazine, the FDG-20 nanozyme was magnetically separated from the reaction mixture and washed with DI water and ethanol and dried in an oven. The recycled catalyst was utilized for the photodegradation of simazine by maintaining the same experimental procedure as stated in section 2.10 (the concentration of simazine: 0.3 mM, catalyst loading: 0.3 g L^{-1} and pH 5). The reusability of the FDG-20 nanozyme has been carried out 12 times by the above similar way.

2.12. Dissolution studies

After performing the photocatalytic degradation of simazine pesticide, the FDG-20 nanozyme was separated by using a magnetic. The dissolution or leaching of iron ions (F^{2+} or Fe^{3+}) in the aqueous part after magnetic separation was analysed by atomic absorption spectrometer (AAS) compared with a standard iron solution.

3. Results and discussion

3.1. Characterization of the synthesized nanomaterials

The X-ray diffraction (XRD) pattern of synthesized GO, DG, FDG-10, FDG-15 and FDG-20 are shown in Fig. 1(a). The diffraction peak at 2θ value of 10.16° disappeared after the functionalization of graphene oxide (DG) and a new diffraction peak at 2θ value of 24.08° corresponds to (002) plane was obtained. The diffraction peaks at 30.12, 35.6, 43.20, 57.36 and 62.94° belong to the (220), (311), (400), (511) and (440) planes of Fe_3O_4 were observed in the FDG-20 nanozyme (JCPDS Card No. 01-075-0449). These diffraction peaks are not clearly observed in FDG-10 and FDG-15 nanozymes. The d-spacing values of (220), (311), (400), (511) and (440) crystallographic planes of FDG-20 nanozyme were calculated by PDXL

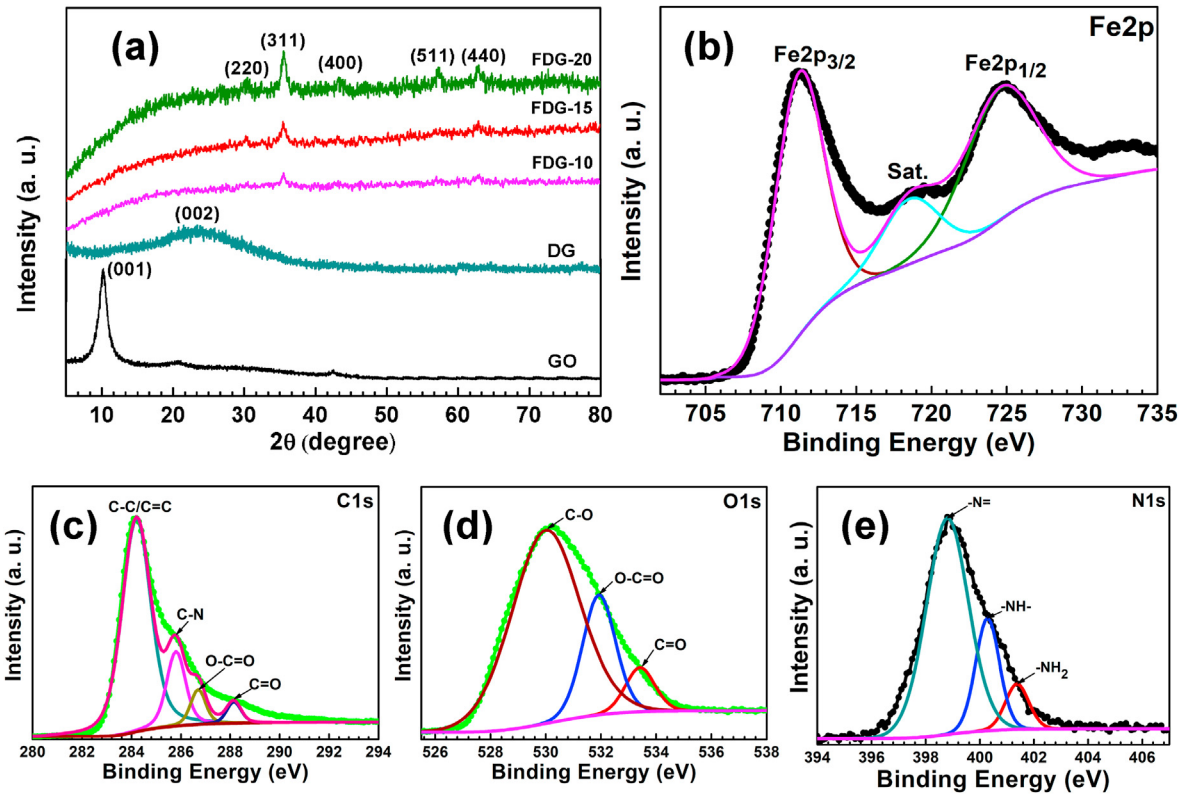

Fig. 1. (a) XRD pattern of GO, DG, FDG-10, FDG-15 and FDG-20 and high-resolution deconvoluted XPS spectrum of (b) Fe 2p (c) C 1s (d) O 1s and (e) N 1s of FDG-20.

software and found to be 2.942, 2.509, 2.08, 1.601 and 1.474 A°, respectively. The disappearance of (002) crystallographic planes after the formation of FDGs nanozyme was observed due to the shielding effect of the strong diffraction peaks of Fe_3O_4 (Chao et al., 2008).

The chemical bonding information and elemental composition of the synthesized nanozyme was examined by X-ray photoelectron spectroscopy (XPS). The survey scans XPS spectra of DG, FDG-20, FDG-10 and FDG-15 are shown in Fig. S2 (ESI). The survey scans XPS spectrum for DG sheets was obtained with three sharp peaks at binding energies of 284.72, 400.21 and 530.22 eV signifying the presence of C, N and O (Fig. S2a). The additional peak at 711.18 eV obtained for FDG-20 nanozyme indicates the occurrence of Fe in the nanozyme. The survey scans XPS spectrum of FDG-10 and FDG-15 were obtained with binding energy peaks similar to the FDG-20 (Figs. S2b and c). The relative atomic percentage obtained from the survey scan spectrum is shown in Table 1. It was observed that, the amount of iron content in the nanozyme increases with increasing iron salt concentration from FDG-10 to FDG-20 during the synthesis. The high-resolution Fe2p XPS spectrum shows two peaks at 711.2 and 724.6 eV corresponds to the spin orbit-splitting of Fe $2p_{3/2}$ and Fe $2p_{1/2}$, respectively representing the formation of a mixed metal oxide of Fe(II) and Fe(III) (Fig. 1(b)). The satellite peak at 718.5 eV is the characteristic of Fe(III) (Ouyang et al., 2014). The high-resolution peak fitting spectrum of C1s was fitted with four different distinct peaks at 284.2, 285.8, 286.7 and 288.15 eV belongs to the C–C/C=C, C–N, O–C=O and C=O bonds of DG (Fig. 1(c)). The deconvoluted high-resolution spectrum of O1s was obtained with three different peaks with binding energy values of 530, 531.9 and 533.2 eV corresponds to the C–O, O–C=O and C=O bonds, respectively (Fig. 1(d)). Similarly, the high-resolution deconvoluted spectrum of N1s shows peaks at 398.8, 400.3 and 401.4 eV were correlated with the –N = , $-NH_2$, –NH– bonds of DG, respectively.

Table 1
Relative atomic percentages of DG, FDG-10, FDG-15 and FDG-20.

Materials	Atomic%			
	C	N	O	Fes
DG	76.89	3.86	19.25	–
FDG-10	40.70	3.27	43.04	12.99
FDG-15	34.80	2.98	44.61	17.61
FDG-20	29.30	0.88	45.93	23.88

The morphology, shape and size of the synthesized nanozymes were examined by transmission electron microscopy (TEM) high-resolution-TEM (HRTEM) analysis as shown in Fig. 2. The distribution size and shape of NPs obtained for FDG-10 (Fig. 2(a,b)) and FDG-15 (Fig. 2(c,d)) are not appropriate as compared to the FDG-20 nanozyme. Well distributed and random shaped NPs were observed for FGD-20 nanozyme (Fig. 2(e,f)). The lattice fringes for Fe_3O_4 NPs are clearly visible in the high-resolution TEM images of FDG-20 (Fig. 2(g)). The lattice fringe spacing of 0.29 nm belongs to the (220) plane of Fe_3O_4. The SAED pattern of FDG-20 nanozyme (inset in Fig. 2(g)) confirms the crystalline nature of the NPs. The average particle sizes of 12 nm are obtained from the distribution curve (Fig. 2(h)), which is determined using image J software. Further, the EDS mapping images in Fig. 2(i-m) show the distribution of C, O, Fe and N elements of FDG-20 nanozyme indicating well distribution of Fe_3O_4 NPs on dopamine functionalized graphene sheets.

The morphology of the synthesized FDG-20 nanozyme was further investigated by atomic force microscopy (AFM) analysis. The topographic unprocessed and processed (20 μm × 20 μm) AFM images of FDG-20 nanozyme is shown in Fig. 3(a and b). The cluster of the well-distributed Fe_3O_4 NPs was observed on DG sheets. The

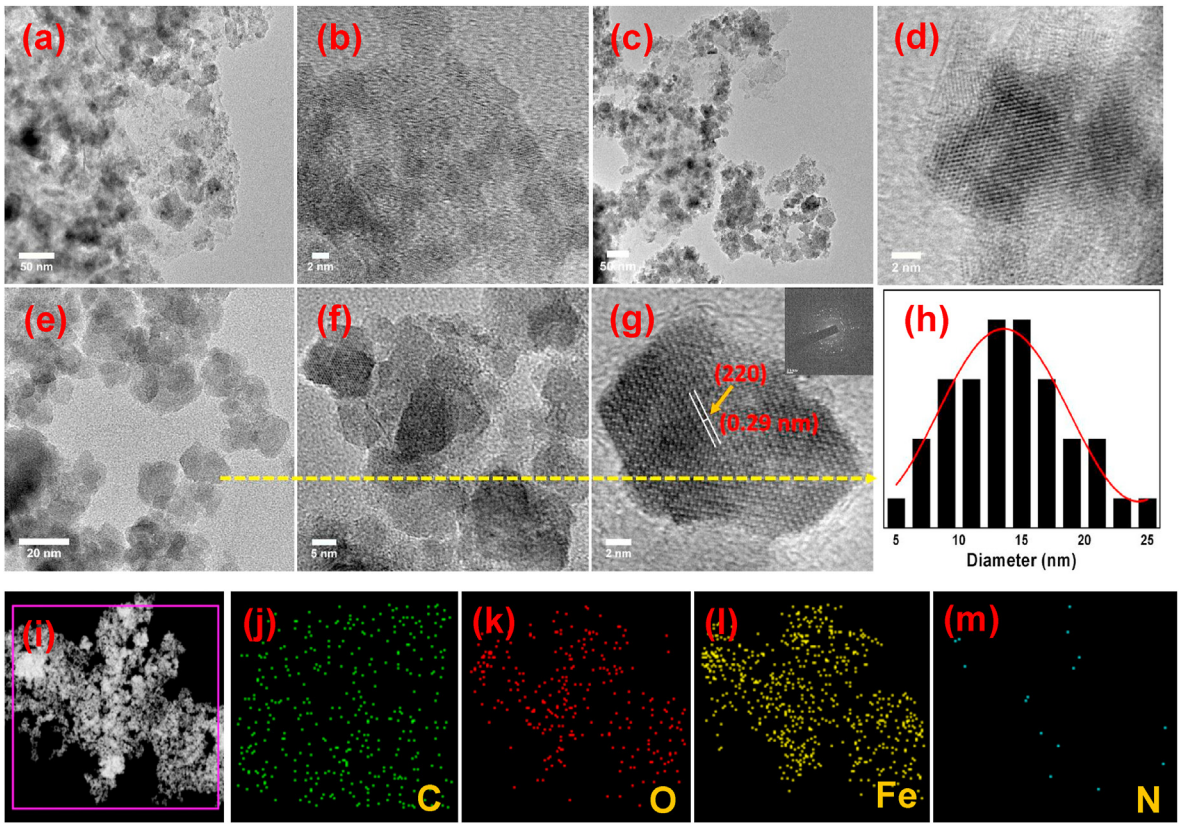

Fig. 2. (a,b) TEM and HRTEM images of FDG-10, (c,d) TEM and HRTEM images of FDG-15 (e,f,g) TEM and HRTEM (inset SAED pattern) images of FDG-20, (f) particle size distribution curve of FDG-20 nanocomposite (average particle size 12 nm) and (i–m) EDS mapping images of FDG-20 nanozyme.

average surface roughness of FDG-20 nanozyme was found to be 33.88 nm. The 3D topographic image of FDG-20 nanozyme signifies good distribution of the NPs on DG sheets Fig. 3(c).

Thermogravimetric (TGA) analysis has been carried out to determine the thermal stability of the FDG-20 nanozyme **(Fig. 3d).** The weight loss was observed gradually from 30 to 800 °C. 14.5% of weight loss up to 200 °C was obtained due to the loss of adsorbed water. Similarly, weight loss (7%) nearby 400 °C was obtained for the loss of functional groups of DG sheets. Moreover, 17.86% of weight loss for the pyrolysis of the carbon skeleton was obtained up to 800 °C. The amount of Fe_3O_4 content in the FDG-20 nanozyme was calculated from TGA weight loss curve, which is found to be 60.64% (Bansal et al., 2015).

Fig. 3(e) shows the room temperature vibrating sample magnetometer (VSM) analysis magnetization hysteresis (M – H) loops of FDG-10, FDG-15 and FDG-20 nanozymes. FDG-10 and FDG-15 nanozymes show weak ferromagnetic behavior. Otherwise, FDG-20 nanozyme showed superparamagnetic behavior. The saturation magnetization values increase from FDG-10 to FDG-20 with increasing Fe_3O_4 content. The saturation magnetization (Ms), coercivity (*Hc*) and remanent magnetization (Mr) values of FDG-20 were obtained as 40.33 emu g^1, 117.79 Oe and 6.03 emu g^1, respectively. Similarly, Ms, Hc, and Mr were found to be 31.58 emu g^1, 110.07 Oe and 4.25 emu g^1 for FDG-10 and 13.16 emu g^1, 210.21 Oe and 1.91 emu g^1 for FDG-15, respectively. Therefore, the FDG-20 nanozyme is easily recoverable using an external bar magnet (inset magnetic separation image) as compared to the FDG-15 and FDG-10 nanozymes.

To understand the interaction of pesticide with the surface of the FDG-20 nanozyme at different pH, it is necessary to investigate the surface charge of the nanocomposite under different pH. It is seen from Fig. 4 that with increasing the pH, the surface charge of FDG-20 nanozyme decreases. At pH 2, the zeta potential value FDG-20 nanozyme was found to be 22 mV whereas, at pH 11, the zeta potential value was found to be −35 mV. The isoelectric point was obtained at pH 5.3, at which the net charge of FDG-20 nanozyme becomes zero. In alkaline medium, ionization of the surface functional groups of FDG-20 nanozyme by OH^- ions occurs which causes the negative surface charges (zeta potential). The accumulation of H^+ ions around the surface of the nanocomposite takes place at acidic medium, which causes the impending of zeta potential values towards positive.

Moreover, the specific surface area of the FDG-20 and our previously reported Fe_3O_4–TiO_2/rGO nanocomposites was calculated using BET isotherms (Figs. S3a and b) (Boruah and Das, 2020). FDG-20 nanocomposite showed a significantly higher surface area of 75.8 m^2 g^{-1} as compared to the Fe_3O_4–TiO_2/rGO nanocomposite (45 m^2 g^{-1}). The additional surface area of FDG-20 nanocomposite must result from the presence of dopamine functionalized graphene (Dong et al., 2014).

3.2. Peroxidase-like activity and establish the FDG as artificial nanozyme

Nanozymes are a collection of nanomaterials that have constituted a group of their own by being able to efficiently mimic the natural enzyme horseradish peroxidase by catalyzing H_2O_2-mediated reaction similar to natural enzymes in shape, size and surface charge and superiority as to how they respond to external stimulus (Manea et al., 2004; Wei and Wang, 2013). The peroxidase-like activity of the desired material can be analysed by a redox reaction caused by the reduction of H_2O_2 and oxidation of a variety of

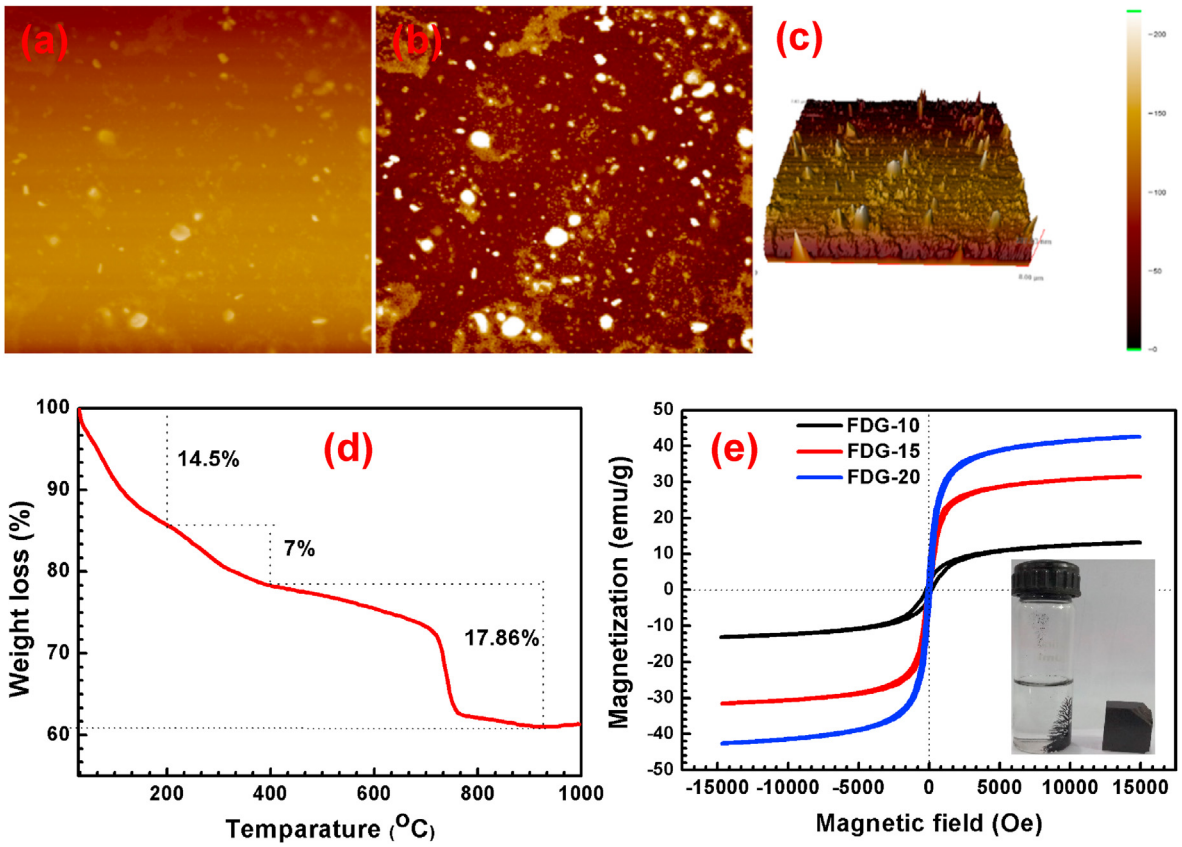

Fig. 3. (a–c) AFM images of FDG-20 (d) TGA analysis of FDG-20 and (e) VSM magnetization hysteresis loops of FDG-10, FDG-15 and FDG-20 nanocomposites.

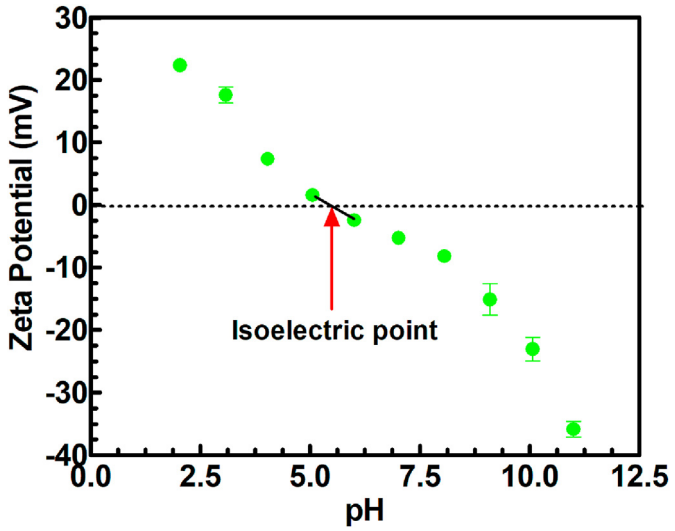

Fig. 4. Zeta potential of FDG-20 nanozyme at different pH (the error bars represents the standard deviation of values for three independent analysis).

chromogenic substrates. TMB is the most-studied chromogen for HRP mimics in acidic conditions as it is less carcinogenic compared to the other studied chromogens (Suhaimy et al., 2016). The enzyme mimetic activity of nanomaterials using TMB-H_2O_2 system can be utilized as a sensing platform that gives a signal detectable by the naked eye. Since the last decade, this detection method using nanozyme has gained sufficient attention amongst young researchers due to its simplicity and ease of operation without the use of sophisticated instruments. In this regard, the functionalized rGO supported composite materials are very suitable, which enhances the interaction between targeted water contaminants and composite materials by π-π interactions.[15]

The TMB oxidation reaction has been carried out to evaluate the peroxidase-like activity of the FDGs nanozyme as shown in Fig. 5(a) (catalyst loading 9 mg L^1 in 0.2 M sodium acetate buffer (pH 4), 0.5 mM TMB and 50 μL of 30% H_2O_2). The FDG-20 nanozyme shows better oxidation capability for the oxidation of TMB than compared to the FDG-10, FDG-15, FDG-20 and DG in the presence of H_2O_2. However, there is no activity of FDG-20 nanozyme towards the oxidation of TMB in the absence of H_2O_2.

The initial pH, temperature and catalyst loading are important parameters in the TMB oxidation reactions. The TMB oxidation reaction has been carried out by varying pH 2 to 11 using FDG-20 nanozyme (0.5 mM TMB, and 50 μL of 30% H_2O_2, catalyst loading 9 mg L^1, temperature 25 °C). The superior catalytic activity was obtained for FDG-20 nanozyme at pH 4 as shown in Fig. 5(b). At pH 2, 9 and 11 no oxidation of TMB was observed. The TMB oxidation reaction was further performed at pH 4 with temperature variation from 25 °C to 55 °C. The TMB oxidation activity of FDG-20 nanozyme decreases with increasing temperature of the reaction medium from 25 °C to 55 °C (Fig. 5(c)). Again, the effect of catalyst loading was studied and executed by varying the catalyst concentration from 1 mg L^1 to 12 mg L^1. Fig. 5(d) shows the TMB oxidation activity of FGD-20 nanozyme at different concentrations. The optimum catalytic activity was achieved with a catalyst loading amount of 9 mg L^1. Therefore, 9 mg L^1 is taken as the optimal catalyst loading concentration for the simazine detection reactions.

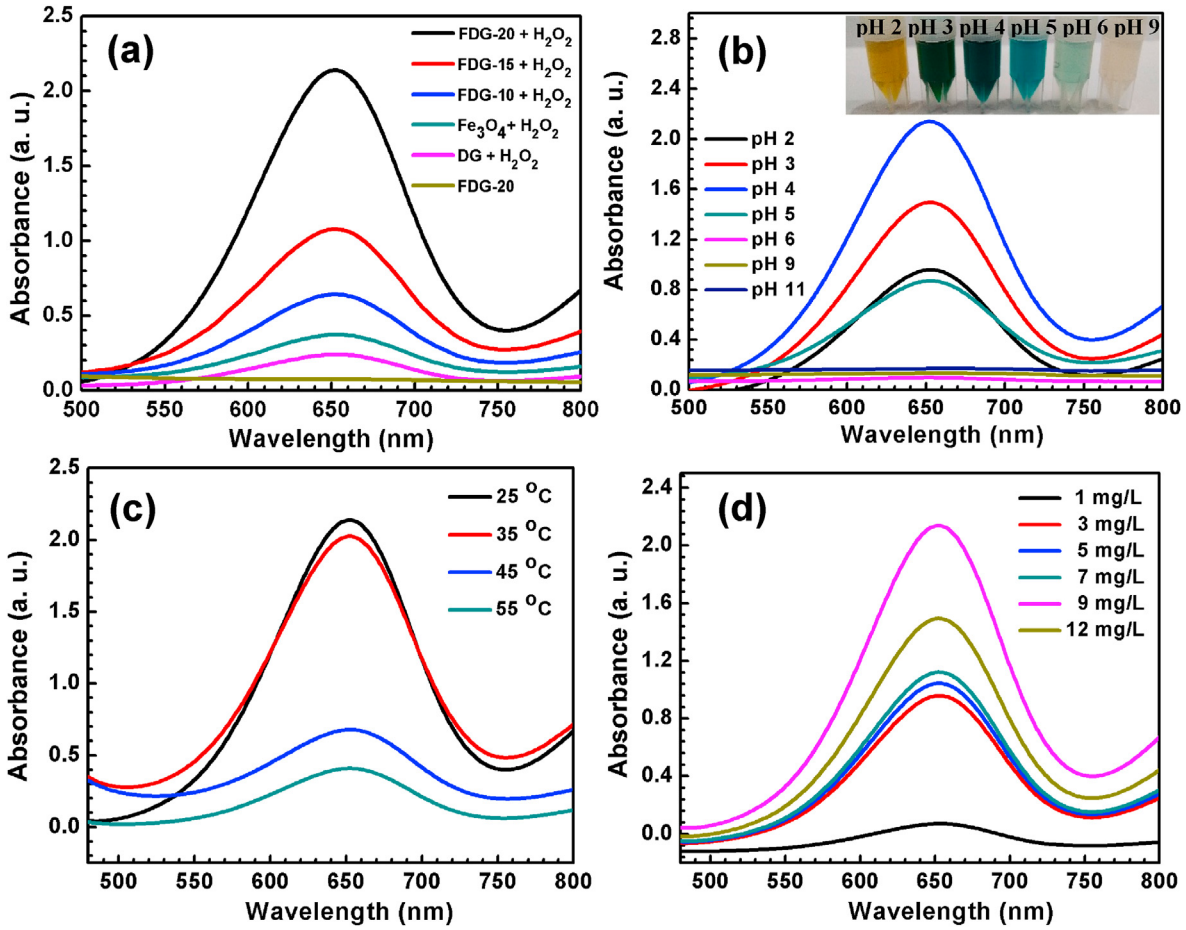

Fig. 5. (a) FDG-20, FDG-15, FDG-10, Fe_3O_4 and DG catalyzing the oxidation of TMB, substrates in the presence of H_2O_2 and UV−vis absorption spectra of TMB in presence of FDG-20 and in absence of H_2O_2 (catalyst loading 9 mg L^{-1}, sodium acetate buffer 0.2 M, 50 μL of 30% H_2O_2 and pH 4), (b) TMB oxidation using 9 mg L^1 of FDG-20 nanocomposite at different pH in sodium acetate buffer (0.2 M, pH 4, 3 mL), 0.5 mM TMB, and 50 μL of 30% H_2O_2, (c) TMB oxidation using 9 mg L^{-1} of FDG-20 at different temperature in sodium acetate buffer (0.2 M, pH 4, 3 mL), 0.5 mM TMB, and 50 μL of 30% H_2O_2, pH 4 and (d) TMB oxidation by varying FDG-20 nanocomposite loading amount in sodium acetate buffer (0.2 M, pH 4, 3 mL), 0.5 mM TMB, and 50 μL of 30% H_2O_2, pH 4.

3.2.1. TMB oxidation kinetics

The steady-state kinetics measurements were executed by varying one of each substrate concentration (H_2O_2 and TMB) and by keeping the other parameters constant as shown in Fig. 6(a and b). The absorbance value at a specific substrate concentration was analysed by applying Beer Lambert's law, which can be written as

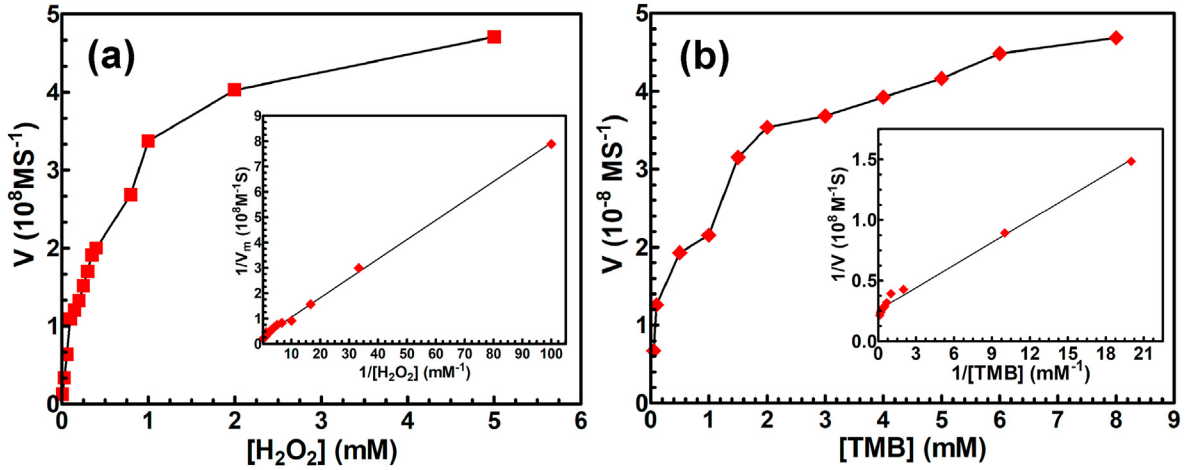

Fig. 6. Steady-state kinetic assay for FGD-20 nanocomposite (a) variation of H_2O_2 concentration (10−400 mM) at constant TMB concentration (0.5 mM), (b) variation of TMB concentration (0.05−8 mM) at constant H_2O_2 concentration (50 mM) (inset the corresponding Lineweaver-Burk plots of the double reciprocal of Michaelis-Menten equation).

Table 2
The maximal velocity (Vm) and Michaelis constant (Km) for synthesized nanomaterials.

Catalysts	Substrates	Km (mM)	Vm (10^{-8} MS^{-1})
FDG-20	H_2O_2	0.089	5.55
FDG-20	TMB	0.242	3.90
FDG-15	H_2O_2	0.287	3.39
FDG-15	TMB	0.298	2.89
FDG-10	H_2O_2	0.302	2.41
FDG-10	TMB	0.313	1.97
Fe_3O_4	H_2O_2	0.355	1.60
Fe_3O_4	TMB	0.373	1.43
DG	H_2O_2	0.585	1.30
DG	TMB	0.626	1.14

$$A = \in_{TMBDI} \times C \times L \quad (3)$$

where A is the absorbance, ε is the molar extinction coefficient (39,000 M^{-1} cm^{-1}), C is the concentration of the substrate and L assigned as path length. Both H_2O_2 and TMB followed the typical Michaelis-Menten model up to a certain concentration range. The maximal velocity (Vm) and Michaelis constant (Km), both are important parameters for the determination of substrate affinity in peroxidase-like reactions. Therefore, the Km and Vm for both H_2O_2 and TMB substrates were determined from Lineweaver-Burk double reciprocal plot as an inset in Fig. 6(a and b). The Km and Vm were found to be 0.089 mM and 5.55 × 10^{-8} for H_2O_2 and 0.242 and 3.90 × 10^{-8} for TMB, respectively. Further, the Km and Vm were determined for DG, Fe_3O_4, FDG-10 and FDG-15 as shown in Table 2. The lower Km of 0.089 mM and 0.242 mM for H_2O_2 and TMB substrates were obtained using FDG-20 nanozyme which represents a high substrate affinity in comparison to other catalysts.

3.2.2. Mechanism of the peroxidase mimics activity

The FDG-20 nanozyme shows maximum peroxidase-like activity due to high Fenton activity in presence of H_2O_2 than compared to the FDG-10 and FDG-15 nanozymes (**Fig. 5a**). The Fenton activity of the FGD-20 nanozyme can be represented by the following reactions. Scheme 2 showing the graphical illustration of peroxidase mimics the activity of FDGs nanozymes. Initially, the TMB molecule was adsorbed onto the FDGs nanozymes surface [step I, Scheme 2]. The role of the functionalized graphene surface for the efficient adsorption of TMB molecules was studied in one of our previous publications (Das et al., 2019). Since, before oxidation, the TMB molecules are necessary to be adsorbed on the nanozymes, the surface functionalization of the graphene sheets using polydopamine affords more adsorption sites for the TMB molecules due to the existence of phenolic hydroxyl and amide groups leading to the enhanced catalytic effect of the FDGs nanocomposite (Han et al., 2014). In the presence of H_2O_2, •OH is produced due to the occurrence of Fenton reaction [step II, Scheme 2]. •OH are accountable for the formation of blue coloured Ox-TMB product, which is rapid equilibrium with the cation free-radicals $TMB^{+\bullet}$ [step III, Scheme 2].

$$Fe^{2+} + H_2O_2 \rightarrow Fe^{3+} + {}^{\bullet}OH + OH^{-} \quad (4)$$

$$Fe^{3+} + H_2O_2 \rightarrow Fe^{2+} + {}^{\bullet}OH_2 + H^{+} \quad (5)$$

$$TMCB = {}^{\bullet}OH \rightarrow O_X - TMB \quad (6)$$

The OH• radical is responsible for efficient TMB oxidation which was confirmed in our reaction by using non-fluorescent TA. TA can combine with •OH and produce a highly fluorescent product 2-hydroxyterephthalic acid (HTA). HTA shows fluorescence emission signal at 425 nm by keeping an excitation wavelength of 415 nm (Fig. 7). The generation of OH• is equivalent to the intensity of the fluorescence emission signals. The maximum fluorescence intensity signal was observed for FDG-20 + H_2O_2 + TA reaction system as shown in Fig. 7(i). Otherwise, the fluorescence intensity signals were gradually decreased for (ii) Fe_3O_4+ H_2O_2 and (iii) FDG-20 + TA reaction systems. The synergistic effect between Fe_3O_4 and functionalized rGO enhances the •OH generation capability of the FDG-20 nanozyme. On the other hand, in the absence of H_2O_2, FDG-20 nanozyme alone did not produce a sufficient amount of •OH, which results in weak fluorescence intensity signals of FDG-20 + TA reaction system (Ivanova et al., 2019).

3.2.3. Sensitivity of FDG-20 nanozyme for detection of simazine

FDG-20 nanozyme achieved excellent peroxidase-like activity towards TMB oxidation reactions as clearly investigated in the previous sections. Based on this finding, FDG-20 nanozyme was efficiently utilized for the sensitive detection of simazine pesticide. Simazine in the drinking water system causes kidney congestion and low blood pressure in human bodies (Agdi et al., 2000; Segura et al., 2007; Clemente et al., 2014). With the FTG-20 nanozyme, UV−visible spectrophotometer can be utilized as a suitable platform for the detection of a pesticide in the pesticide containing

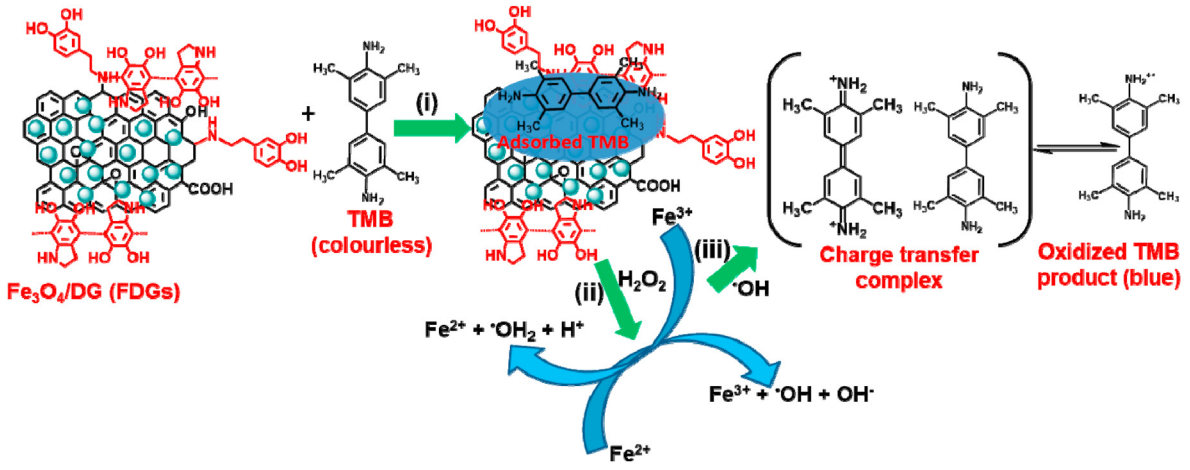

Scheme 2. Scheme showing the graphical representation of peroxidase mimics activity of FDGs nanozyme as (i) TMB adsorption onto FDGs nanozyme (ii) generation of •OH and (iii) oxidation of TMB by •OH.

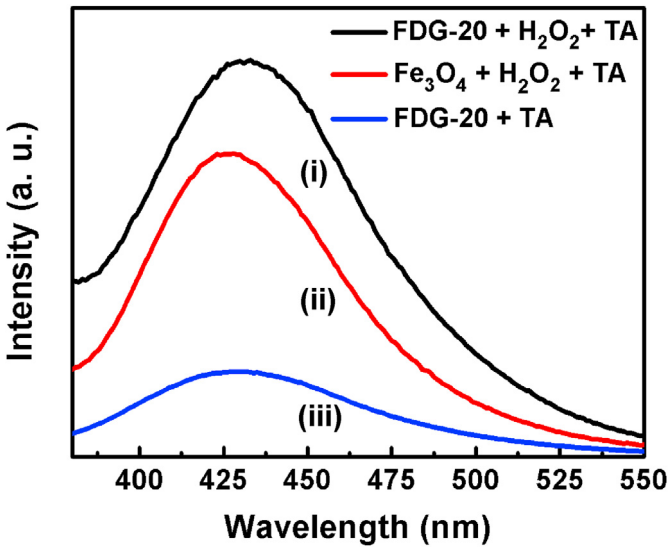

Fig. 7. Fluorescence emission spectra of (i) FDG-20 + H_2O_2 + TA, (ii) Fe_3O_4+ H_2O_2 + TA and (iii) FDG-20 + TA.

wastewater. For the experiment, different concentrations of freshly prepared simazine (0.01–90 μM) were allowed to react with 0.5 mM TMB solution in 0.2 M sodium acetate buffer solution (2.5 mL, pH 4) followed by the addition of 50 μL H_2O_2 solution and 9 mg L^{-1} catalysts and the total volume was adjusted to 5 mL by adding buffer solution. The final reaction mixture was incubated for 30 min at 25 °C. The changes in the intensities at a wavelength of 652 nm due to ox-TMB (blue color) were studied by changing the concentration of simazine using a UV–visible spectrophotometer. Following this a calibration curve was constructed by plotting absorbance at 652 nm versus different concentrations of simazine. With the increase in the concentration of simazine, the absorbance decreased accordingly. The hydrogen bonding between simazine and TMB molecules causes inhibition of the TMB oxidation (Wu et al., 2008). Scheme S1 (ESI) shows the hydrogen bonding interactions between simazine and TMB. The calibration curve of the peak absorbance value at 652 nm in the concentration range of 0.01 μM–50 μM is shown in the inset of Fig. 8(b). However, the linearity of the system is start from 2.3 μM after the plateau region at low concentrations and end at 50 μM simazine concentrations Fig. 8(b). Thus, the LOD is readable from the graphs. The fitting equation to the concentration range where linearity prevails is a polynomial first-order. The linear fitting equation is Y = mx + b. The non-linear portions of the plot are not considered. Where substitute the measured value as x into the equation and solve for Y. The m and b are the slope and y-intercept, respectively. Similarly, Ma et al. and Qiao et al. were calculated LOD values of 1.39 μM and 1.136 nM for the detection of glucose using carbon nanotube

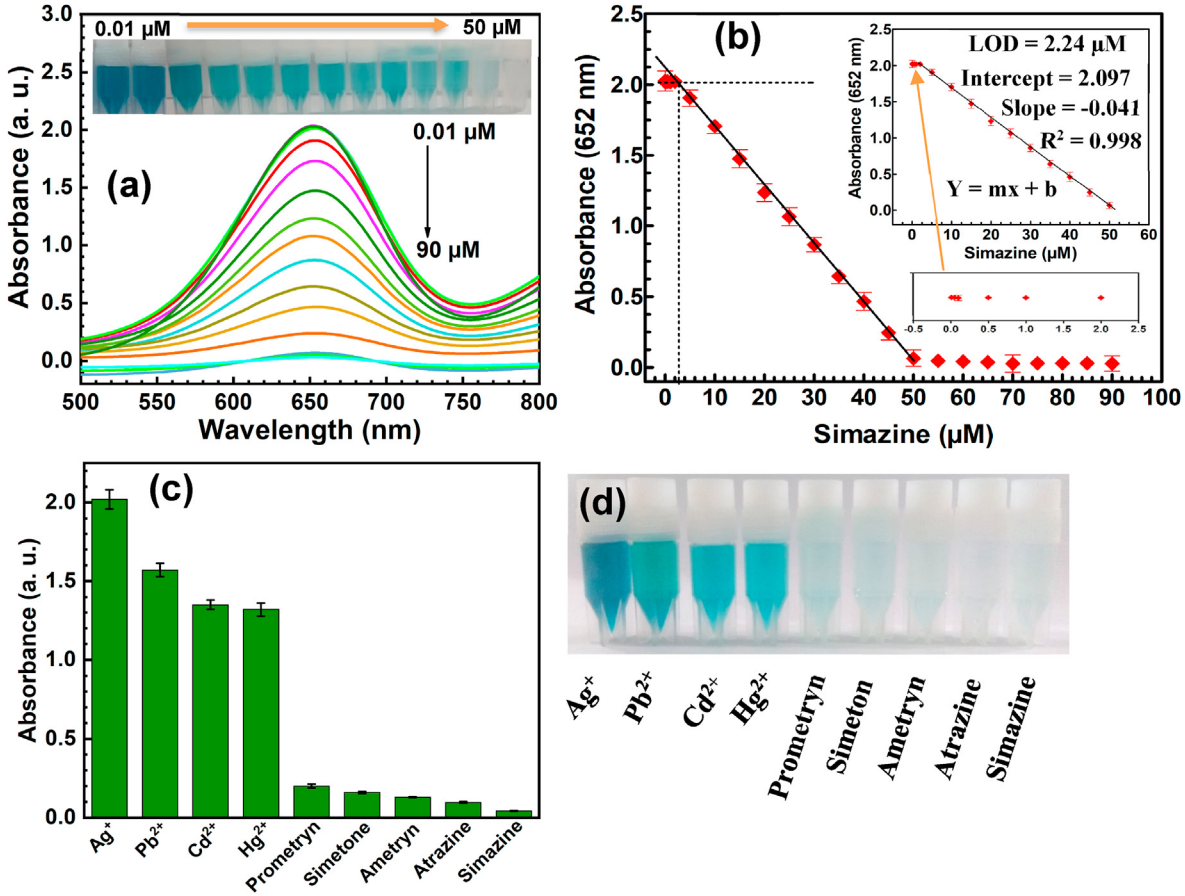

Fig. 8. (a) UV–visible spectra of the Ox-TMB product in presence of different concentrations (0.01 μM–90 μM) of simazine (0.5 mM TMB in acetate buffer (0.2 M, pH 4, 3 mL), 50 μL of 30% H_2O_2 and FDG-20 loading: 9 mg L^{-1}), (b) plot of the absorbance values versus different concentration of simazine at 652 nm (inset corresponding calibration plots of the reaction system at concentration range 0.01 μM–50 μM and the magnification of plateau region) (c) bar diagram showing the selectivity study of triazine pesticides detection using FDG-20 nanocomposite in presence of different interfering ions and pesticides and (d) the corresponding TMB oxidation photos (the error bars in Fig. 8(b and c) represents the standard deviation of values for three independent analysis).

supported silver NPs and FeSe−Pt@SiO_2 nanospheres, respectively (Ma et al., 2017; Qiao et al., 2015).

Although our previous publication focuses on the detection and degradation of atrazine pesticide using mixed metal oxide/graphene (Fe_3O_4−TiO_2/rGO) composite materials (Boruah and Das, 2020). However, the nanocomposite material reported in this currently submitted publication is far novel and different in several aspects such as low temperature and less time-consuming synthesis process, increase in the surface area of the nanocomposite due to functionalization as well as high sensitivity towards detection of simazine pesticide. In our previous work, TiO_2, which is one of the most widely used semiconductors (band gap 3.0−3.2 eV) played a vital role in the degradation of atrazine pesticide. However, TiO_2 possesses several disadvantages like poor adsorption, rapid recombination of electron-hole pair and low surface area (Mohamed, 2019). In contrast to our previous work, an efficient detection limit and degradation was achieved in this work using only graphene functionalized Fe_3O_4 nanocomposites without using TiO_2. Slightly better LOD of 2.24 μM (Fig. 8(a,b)) was observed for simazine detection using FDG-20 nanozyme as compared to the Fe_3O_4−TiO_2/rGO nanocomposite with the LOD of 4.85 μM (Figs. S4a and b), which signifies the better catalytic efficiency of the FDG-20 nanozyme. The LOD for simazine detection using Fe_3O_4−TiO_2/rGO nanocomposite was also determine from the linear plot (inset in Fig. S4b) in the concentration range 0.01−50 μM. However, proper linearity was observed from 4.9 μM concentrations. Thus, the LOD of 4.85 μM was obtained for simazine detection using Fe_3O_4−TiO_2/rGO nanocomposite.

The selectivity of the FDG-20 nanozyme towards simazine detection was investigated in the presence of different triazine pesticides and interference inorganic ions like Ag^+, Pb^{2+}, Cd^{2+} and Pb^{2+} ions. From the UV−visible absorbance changes at 652 nm for Ox-TMB, it was observed that the absorbance intensity decreases in the presence of triazine pesticides (Fig. 8(c)). The absorbance intensity slightly decreases in presence of Pb^{2+}, Cd^{2+} and Hg^{2+} ions, but the blue color of the Ox-TMB exists in the reaction mixture (Fig. 8(d)). The interference studies were also carried in presence of four different commonly used organophosphorus pesticides such as Malathion, Chloropyrifos, Dibrom and Methidathion. The UV−visible absorbance intensity at 652 nm for Ox-TMB decreases in presence of these organophosphorus pesticides (Fig. S5). However, the blue color of the Ox-TMB exists in the reaction mixtures. Further, no significant changes were observed in existence of Ag^+, Pb^{2+}, Cd^{2+} and Hg^{2+}, Malathion, Chloropyrifos, Dibrom and Methidathion even after increasing their concentration up to 5 times. Therefore, our designed sensor selectively worked toward the detection of triazine pesticides.

3.2.4. Detection of simazine in spiked environmental samples

The practical applicability of the FDG-20 nanozyme was investigated by the detection of simazine in different spiked water samples (Table 3). The recovery of simazine from the environmental water samples was found to be 94.5%−99%, which indicates that our synthesized nanozyme efficiently works for the pesticides detection in spiked environmental samples.

3.3. Photocatalytic activity of FDG nanozyme towards the degradation of pesticides

After detection, the removal of organic pollutant molecule from the aqueous medium is extremely important to overcome the shortcoming issue of water in worldwide. The photocatalytic process is highly efficient for the decomposition of organic pollutant molecules to non-toxic molecules and ions. The photocatalytic activity of the FGD-10, FGD-15 and FGD-20 nanozymes was investigated towards the degradation of simazine pesticide under sunlight irradiation. Fig. 9(a) shows the changes of UV−visible spectra for the degradation of simazine using FDG-20 nanozyme under sunlight irradiation at a different time interval. The intensity of the absorbance peak at 221 nm decreased gradually with increasing irradiation time. Maximum simazine degradation (97%) was obtained in 50 min of sunlight irradiation (catalyst loading 0.3 g L^{-1}, the concentration of simazine 0.3 mM and pH 5).

Fig. 9(b) shows the comparative degradation of simazine executed using GO, DG, Fe_3O_4, FDG-10, FDG-15 and FDG-20 and in the absence of a catalyst under irradiation of sunlight (catalyst loading: 0.3 g L^1, concentration of simazine: 0.3 mM and pH 5). The FDG-20 showed maximum degradation capacity (97%) in comparison to the GO, DG, Fe_3O_4, FDG-10 as FDG-15 as 33%, 34%, 39%, 51% and 68%, respectively. Otherwise, only 3% of simazine degradation was obtained in the absence of catalyst within 55 min under irradiation of natural sunlight. Since, Fe_3O_4 behaves as a semiconductor, which is activated under irradiation of sunlight. Further activation of Fe_3O_4 NPs was perceived in the presence of DG sheets. Therefore, maximum simazine degradation was obtained using FDG-20 nanozyme. Similarly, the degradation of simazine was executed in the presence of four different light sources such as sunlight, visible light, solar light and UV-light and in dark under same experimental conditions (Fig. 9(c)). The highest simazine degradation efficiency was obtained in the presence of direct natural sunlight sources. However, 90%, 73% and 63% simazine degradation were observed under visible light, solar light and UV-light irradiation. Otherwise, only 31% simazine adsorption onto FDG-20 nanozyme was observed in dark.

Similarly, the FDG-20 nanozyme was utilized towards the photocatalytic degradation of another four different triazine pesticides such as simetone, atrazine, ametryn and prometryn under irradiation of natural sunlight (catalyst loading: 0.3 g L^{-1}, concentration of pesticides: 0.3 mM and pH 5). The FDG-20 nanozyme showed 89%, 87%, 95% and 92% photodegradation efficiencies for the simetone, atrazine, ametryn and prometryn pesticides degradation, respectively. Thus, the synthesized FDG-20 nanozyme is very

Table 3
Recovery of simazine in environmental samples.

Sample	Spiking concentrations (μM)	Obtained concentrations (μM)	RSD (%)	Recovery (%)
River water	30	28.6	3.38	95.34
	40	39	1.79	97.50
	50	49.5	0.71	99.00
Tube well	30	29	2.40	96.67
	40	38.7	2.34	96.75
	50	48.9	1.57	97.8
Pond water	30	29.6	0.95	98.67
	40	37.8	4.00	94.50
	50	49.5	0.71	99.00

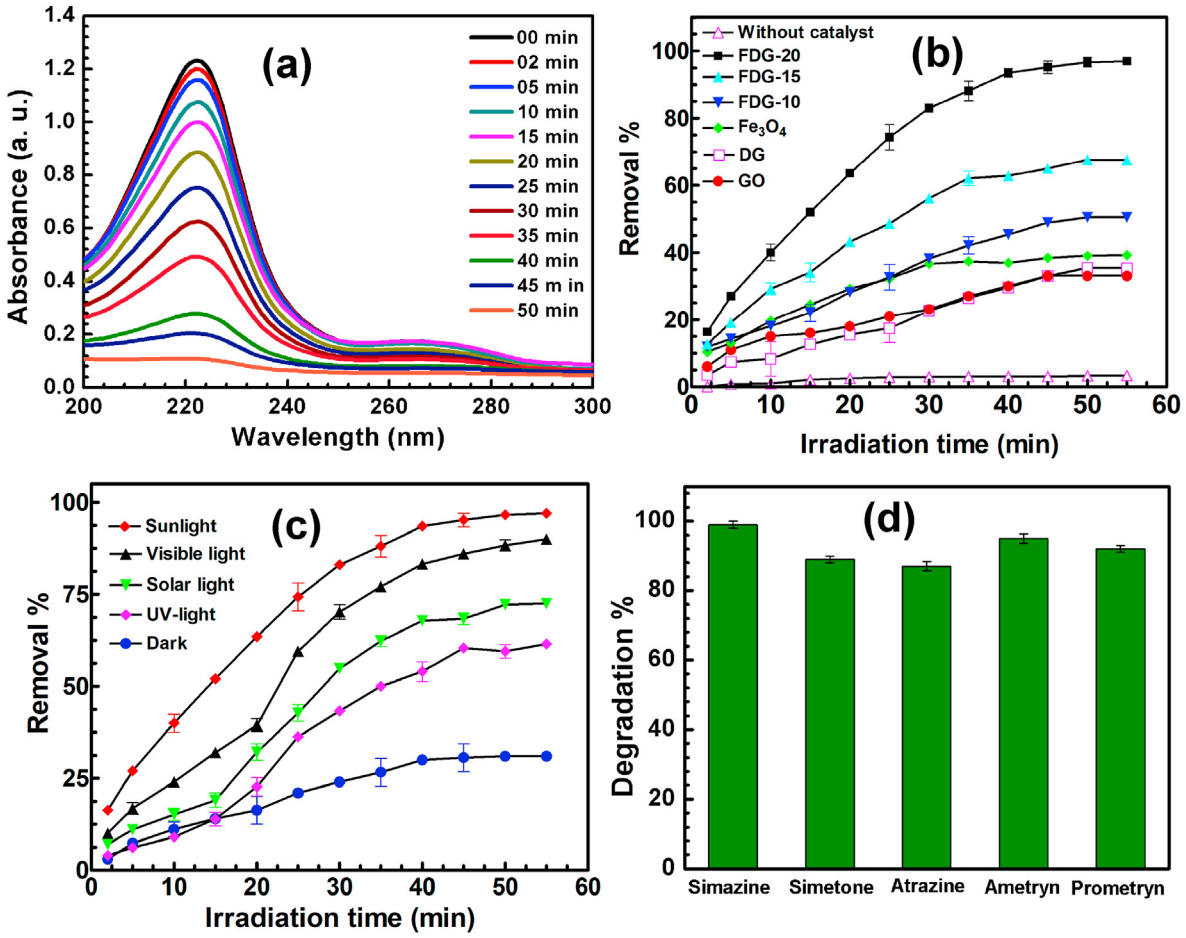

Fig. 9. (a) UV–Visible spectral changes for the photocatalytic degradation of simazine; (b) comparative simazine removal using GO, DG, Fe_3O_4, FDG-10, FDG-15, FDG-20 and in absence of catalyst under sunlight irradiation (catalyst loading: 0.3 g L^{-1}, concentration of simazine: 0.3 mM and pH 5); (c) simazine degradation in presence of different light sources (catalyst loading: 0.3 g L^{-1}, concentration of simazine: 0.3 mM and pH 5) and (d) comparative photocatalytic degradation of five different triazine pesticides using FDG-20 nanocomposite under sunlight irradiation. (The error bars in all figures represents the standard deviation of values for three independent analyses).

suitable for the photocatalytic degradation of different triazine pesticides in an aqueous medium. The FDG-20 nanozyme showed superior photocatalytic efficiency as compared to the most of the previously reported photocatalysts within a shorter time period (50 min) as presented in Table 4. As reported in our previous publication, a photocatalytic degradation efficiency of 90% towards atrazine was obtained using Fe_3O_4–TiO_2/rGO, whereas a much high degradation efficiency of 97% was obtained towards simazine using FDG-20 nanozyme (Boruah and Das, 2020). This effect could be attributed to the functionalization of the graphene sheets using the dopamine moieties that lead to the generation of higher surface area and ultimately towards higher adsorption of simazine on the photocatalyst surface.

The initial concentration of pesticides has significant effect on the degradation process, which is investigated by varying the initial concentration of simazine from 0.1 mM to 0.7 mM as shown in Fig. 10(a) (catalyst loading: 0.3 g L^{-1} and pH 5). The photodegradation efficiency of FDG-20 nanozyme decreases gradually with increasing initial concentration of simazine. However, almost similar degradation efficiency of 97% and 98.6% was observed for 0.3 mM and 0.1 mM initial simazine concentrations. Therefore, 0.3 mM simazine concentration was the optimum concentration for other degradation experiments. The active sites on the catalyst surface decrease with increasing initial pesticide concentration

Table 4
The comparison of the photocatalytic simazine degradation activity of FDGs nanozyme with the reported nanomaterials.

Nanomaterials	Light sources	Irradiation time	Photodegradation (%)	References
Cu/TiO_2 nanotube	UV light	240 min	64	Garg and Bisht (2016)
TiO_2 nanotube	UV light	240 min	60	(Suhaimy et al., 2018)
TiO_2 NPs suspension	Visible light	20 min	95.4	(Rao and Chu, 2013)
TiO_2 NPs	UV light	25 min	~ 95	(Chu et al., 2009)
Diatomite/Zero-valent iron	———	180 min	100	(Sun et al., 2013)
TiO_2–Fe_3O_4/rGO nanocomposite	Sunlight	40 min	90	(Boruah and Das, 2020)
FDG-10	Sunlight	50 min	51	Present work
FDG-15	Sunlight	50 min	68	Present work
FDG-20	Sunlight	40 min	97% (99% at pH 3)	Present work

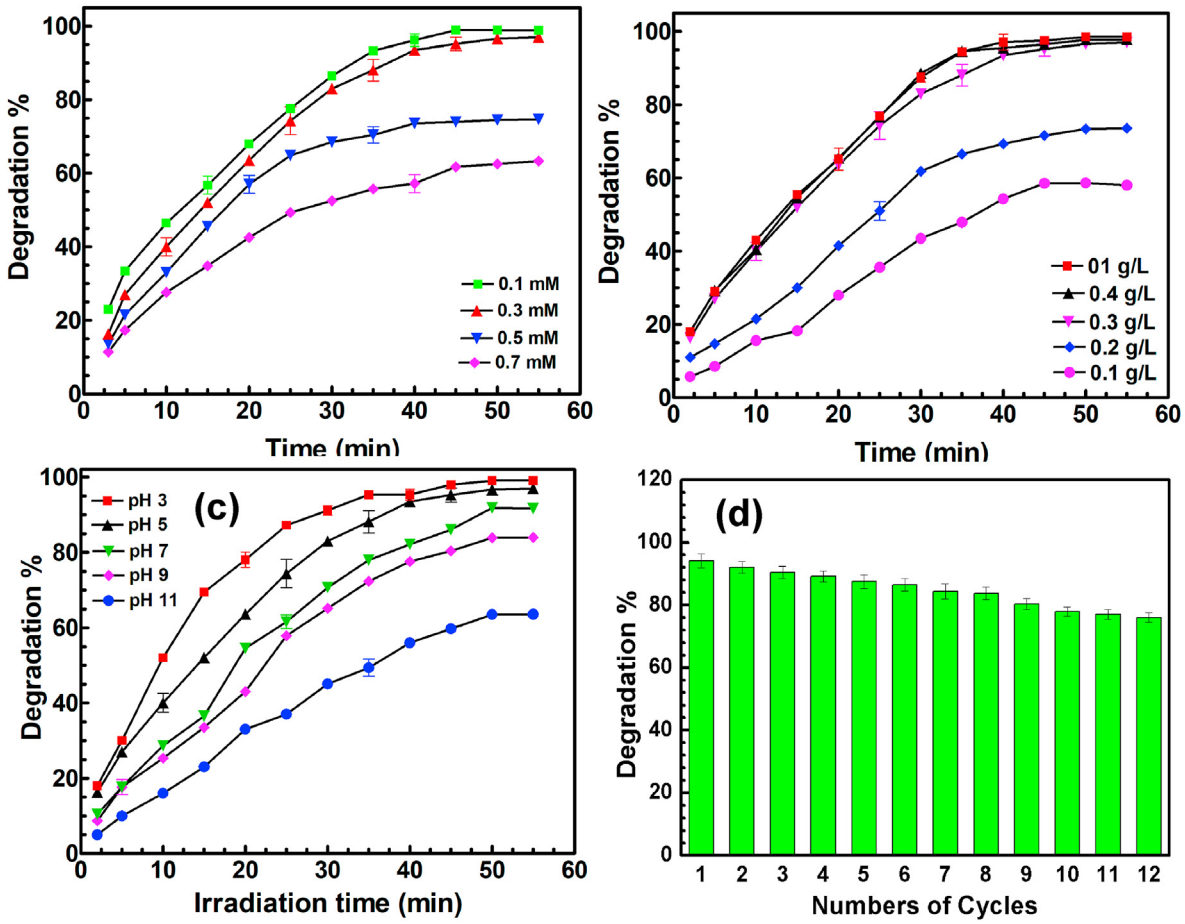

Fig. 10. Photocatalytic degradation of simazine by (a) effect of varying initial simazine concentration (catalyst loading 0.3 g $L^{-1}$and pH 5); (b) effect of varying catalyst loading amount for simazine degradation (concentration of simazine: 0.3 mM and pH 5); (c) effect of varying initial pH (concentration of simazine: 0.3 mM) (inset pseudo first-order kinetic model at different pH) and (d) reusability studies. (The error bars in all figures represents the standard deviation of values for three independent analyses).

which results in decreased degradation efficiency.

The catalyst loading effect on the photocatalytic degradation of simazine was studied under irradiation of natural sunlight at fixed pH 5 (Fig. 10(b)). The photodegradation of simazine was increased with increasing catalyst concentration up to 0.3 g L^{-1}. After that, the simazine degradation efficiency almost remains same up to 5 g L^{-1}, which results in the overlapping of active sites of the catalyst with increasing catalyst concentration.

The initial solution pH also interferes with the photocatalytic degradation process. Thus, simazine degradation was studied by varying initial pH (3–11) as shown in Fig. 10(c). The accumulation of H^+ ions around the surface of the nanocomposite takes place in acidic medium (Fig. 4, zeta potential). Thus, the degradation efficiency decreases with increasing initial pH and the maximum simazine degradation efficiency was observed at pH 3 (99%) and it decreased to 64% when the initial pH of the solution was taken 11. The oxygen functionalities of DG sheets were deprotonated as well as dissolved in a highly basic aqueous medium. Therefore, the interaction between pesticides and photocatalyst is restricted to basic medium and due to this fact, the maximum simazine degradation was attained in acidic pH (pH 3). The kinetics of simazine photodegradation was investigated at different initial pH as an inset in Fig. 10(c). The kinetics results of the simazine degradation were well fitted with a Langmuir-Hinshelwood pseudo-first order kinetic model, which can be represented by the following equation.

$$In(C_0 / C) = kt \quad (7)$$

Where, C_o and C *are* the initial concentration and concentration of simazine at time t, respectively. a k is the rate constant (min^{-1}), respectively. The rate constant and different kinetic parameters were calculated by using the above equation and presented in Table 5.

The recycling test of the catalyst after performing the reactions is very essential for their useful applications. Reusability studies also determine the stability and sustainability of the catalyst. The reusability of the FDG-20 nanozyme has been carried out 12 times under irradiation of natural sunlight as shown in Fig. 10(d) (the concentration of simazine: 0.3 mM, catalyst loading: 0.3 g L^{-1} and pH 5). The photocatalytic degradation efficiency decreases gradually from the first cycles (94%) to the 12 cycles (76%) due to the loss of very fine particles and slight dissolution (0.12 mg) of iron ions at

Table 5
Kinetics model parameters for the photodegradation of simazine.

Substrate	pH	K (min^{-1})	Degradation (%)	R^2
Simazine	3	0.0921	99	0.996
	5	0.0701	97	0.976
	7	0.0501	92	0.978
	9	0.0365	84	0.990
	11	0.0202	64	0.995

pH 5 during the photocatalytic degradation process. Therefore, FDG-20 nanozyme can be repeatedly used for numerous times with abundant activity.

3.3.1. Mechanism of the photocatalytic simazine degradation

Fe_3O_4 is an indirect band gap (1.4 eV) semiconductor, which have high electron-hole pair recombination property. Graphene sheets have high optical properties. Therefore, graphene sheets enhance the light absorption properties of Fe_3O_4 NPs as well as it acts as an electron carrier from the CB to its surface. The functionalization of graphene sheets by dopamine enhances the interaction of graphene sheets with the pesticide molecules. Further, DG sheets have high electron carrier capabilities through its π-bonding network results in the high photocatalytic activity of FDGs nanozyme. Under light irradiation, FDGs nanozyme absorbs a photon and a redox reaction takes place by the promotion of an electron from the valence band (VB) to the CB (Eq^n 8). The electron in the CB can be easily transferred to the DG surface creating a hole in the VB (Eq^n 8). An electron on the DG surface simultaneously captures dissolved molecular oxygen and results in the formation of superoxide radical anion ($O^{\bullet}_2^-$) (Eq^n 9). The superoxide radical anions directly come in interact with water molecules to form $^{\bullet}OH$ (Eq^n 10–12). Similarly, holes (h^+) can contact with water molecules producing $^{\bullet}OH$ (Eq^n 13). The $^{\bullet}OH$ decomposes the simazine pesticides to non-toxic inorganic molecules and ions (Eq^n 14). The schematic representation for the simazine degradation is shown in Scheme 3.

$$FDG(Fe_3O_4) + h\nu \rightarrow Fe_3O_4(h^+) + DG(e^-) \quad (8)$$

$$DG(e^-) + O_2 \rightarrow DG(e^-) + O^{\bullet}_{2^-} \quad (9)$$

$$O^{\bullet}_{2^-} + H_2O \rightarrow HO^{\bullet}_2 + OH^- \quad (10)$$

$$DG(e^-) + HO^{\bullet}_2 + H^+ \rightarrow H_2O_2 \quad (11)$$

$$DG(e^-) + H_2O_2 + H^+ \rightarrow {}^{\bullet}OH + H_2O \quad (12)$$

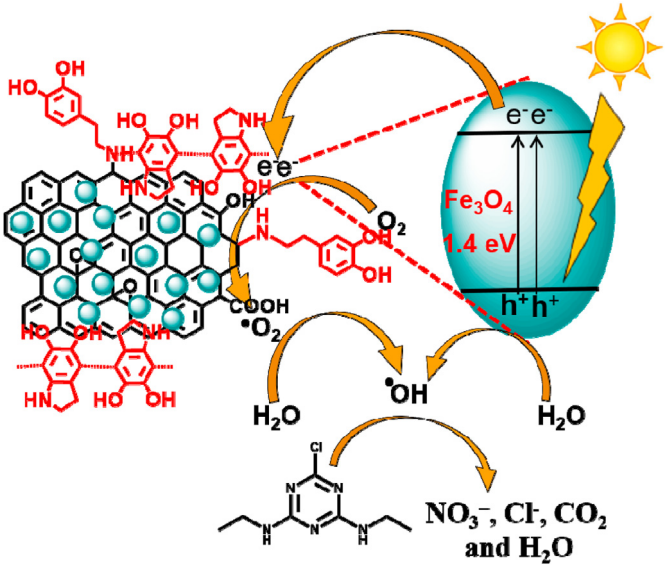

Scheme 3. Schematic illustration showing the photocatalytic degradation of simazine using FDGs nanozyme under irradiation of natural sunlight.

$$Fe_3O_4(h^+) + OH^- \rightarrow Fe_3O_4 + {}^{\bullet}OH \quad (13)$$

$$\text{Simazine} + OH^{\bullet} \rightarrow (CO_2, H_2O, Cl^- \text{and } NO_3{}^-) \quad (14)$$

To support the simazine photodegradation mechanism, we have studied the effect of scavengers during the degradation of simazine under irradiation of natural sunlight. Thus, the degradation of simazine was investigated in presence of each 0.3 mM benzoquinone and isopropanol to quench $O^{\bullet}_2^-$ and $OH^{\bullet}$, respectively. The photodegradation activity of FDG-20 nanozyme decreased in the presence of benzoquinone and isopropanol as a scavenger (Fig. S6). The photodegradation activity of FDG-20 nanozyme was found to be 56% and 47% within 1 h in presence of benzoquinone and isopropanol scavengers, respectively. The above studies confirm that the $O^{\bullet}_2^-$ and $^{\bullet}OH$ were produced during the photodegradation of simazine.

3.3.2. Characterization of FDG-20 nanozyme after photocatalytic degradation

The changes related with the crystallinity, surface morphology and chemical states of the FDG-20 nanozyme after photocatalytic reaction were studied by characterizing with XRD, TEM and XPS techniques. The XRD patterns of Fe_3O_4/AG nanocomposite after degradation of simazine is shown in Fig. S7. The peaks belong to the (220), (311), (400), (511) and (440) planes of FDG-20 nanozyme remain unchanged after 12 times used in the photocatalytic simazine degradation. Thus, there is no significant change in the crystallinity of the FDG-20 nanozyme after the photocatalytic degradation process.

Fig. S8 shows the TEM image of FDG-20 nanozyme after the photocatalytic process and it is noticed that Fe_3O_4 NPs is slightly agglomerated on DG sheets after 12 times used in photocatalytic degradation of simazine. However, the TEM image reveals the presence of spherical shaped NPs like the TEM images of the fresh catalyst (Fig. 2(e)). The lattice fringe distance of 0.25 nm belongs to the (311) plane of Fe_3O_4 NPs is observed in the reused FDG-20 nanozyme as shown in Fig. S8(b). Therefore, FDG-20 nanozyme retains the crystalline property even after 12 times used in the photocatalytic degradation.

Moreover, the high-resolution XPS spectra of Fe2p, C1s, O1s and N1s are shown in Figs. S9(a,b,c,d). The XPS results of the used FDG-20 nanozyme are similar to the freshly prepared FDG-20 (Fig. 1(b,c,d,e)). Thus, the chemical state of the FDG-20 nanozyme remains unchanged after used in photocatalytic degradation of simazine.

3.3.3. Dissolution of iron during the photocatalytic degradation

The dissolution iron ions in aqueous solution were studied at pH 3, 5, 7, 9 and 11. The dissolution of 0.17 mg and 0.12 mg of iron from FDG-20 nanozyme was observed at pH 3 and pH 5, respectively. Otherwise, no dissolution of iron was detected at pH 7, 9 and 11. This may be due to the protonation of an oxygen atom from Fe_3O_4 occurs at acidic pH (Panias et al., 1996). Therefore, the slight loss of iron ions was detected in AAS at pH 3 and pH 5, respectively. As the concentration of H^+ ions is decreased with increasing the pH, there is low possibility, if any, for iron ions dissolving in alkaline pH (9-11).

4. Conclusion

In summary, we prepared magnetic Fe_3O_4 NPs on the surface of polydopamine functionalized rGO sheets and established them as an artificial nanozyme. The synthesized nanozymes were successfully utilized towards the colorimetric detection and photocatalytic

degradation of harmful pesticide, simazine. Synthesized nanozymes were first utilized towards peroxidase mimetic activity for the oxidation of TMB to ox-TMB. Based on this catalytic activity, we could determine the presence of the pesticide in an aqueous medium with LOD of 2.24 μM and a wide detection range up to 50 μM. After its detection, the simazine can be removed from the aqueous medium through the photocatalytic degradation process with a maximum degradation or removal efficiency of 99%. The capability to magnetically recover the photocatalyst added to the benefit of catalyst separation after the photocatalytic reactions. Moreover, our developed nanozyme along with magnetic separability could be repeatedly reused up to 12 continuous cycles. No significant loss in the photocatalytic activity of the FDG-20 nanozyme was observed for simazine degradation, which indicates that the catalyst is highly sustainable. The synthesized FDG-20 nanozyme achieved excellent photocatalytic activity for simazine degradation in comparison to most of the reported photocatalysts (Table 4). The synergistic reinforcement effect of the polydopamine functionalized graphene sheets and magnetic Fe_3O_4 NPs, FDGs nanozymes will act as potent next-generation functional nanozyme with improved detection and degradation performance.

Credit author statement

Purna K Boruah: Conceptualization and execution of the experiments, synthesis and characterization of the materials, photocatalytic application experiments, analyisis of the experimetal data, writting original draft of the manuscript.

Gitashree Darabdhara: Execution of the experiments for colorimetric detection section and finalized the selectivity of the detection section.

Manash R Das: Conceptualization, Supervision, finalization of the experimental data, Validation of the data, organization of the prepartion of the manuscript, reviewing the manuscript, editing of the paper, finalization and communication of the manuscript.

Declaration of competing interest

The authors declare that they have no known competing financial interests or personal relationships that could have appeared to influence the work reported in this paper.

Acknowledgement

The authors acknowledged Director, CSIR-NEIST, Jorhat for facilities to carry out the work. Authors acknowledged to Council of Scientific and Industrial Research (CSIR), Indiafor financial support (Project No. MLP 1013 and OLP-2023). Finally, acknowledged SAIF, CSIR-NEIST, Jorhat India for instrument facilities.

Appendix A. Supplementary data

Supplementary data to this article can be found online at https://doi.org/10.1016/j.chemosphere.2020.129328.

References

Agdi, K., Bouaid, A., Esteban, A.M., Hernando, P.F., Azmani, A., Camara, C., 2000. Removal of atrazine and four organophosphorus pesticides from environmental waters by the diatomaceous earth-remediation method. J. Environ. Monit. 2, 420–423.

Akbarzadeh, A., Samiei, M., Davaran, S., 2012. Magnetic nanoparticles: preparation, physical properties, and applications in biomedicine. Nanoscale Res. Lett. 7, 144–156.

Avinash, M.B., Subrahmanyam, K.S., Sundarayya, Y., Govindaraju, T., 2010. Covalent modification and exfoliation of grapheneoxide using ferrocene. Nanoscale 2, 1762–1766.

Bai, H., Liu, Z., Liu, L., Sun, D.D., 2013. Large-Scale production of hierarchical TiO_2 nanorod spheres for photocatalytic elimination of contaminants and killing bacteria. Chem. Eur J. 9, 3061–3070.

Bansal, A., Kumar, A., Kumar, P., Bojja, S., Chatterjee, A.K., Ray, S.S., Jain, S.L., 2015. Visible light-induced surface initiated atom transfer radical polymerization of methyl methacrylate on titania/reduced graphene oxide nanocomposite. RSC Adv. 5, 21189–21196.

Bonansea, R.I., Am, M.V., Wunderlin, D.A., 2013. Determination of priority pesticides in water samples combining SPE and SPME coupled to GC-MS. A case study: suquıa river basin (Argentina). Chemosphere 90, 1860–1869.

Boruah, P.K., Das, M.R., 2020. Dual responsive magnetic Fe_3O_4-TiO_2/graphene nanocomposite as an artificial nanozyme for the colorimetric detection and photodegradation of pesticide in an aqueous medium. J Hazards Matter 385, 121516–121533.

Chao, X., Wang, X., Zhu, J., 2008. Graphene-metal particle nanocomposites. J. Phys. Chem. C 112, 19841–19845.

Chen, Q., Wei, W., Lin, J.-M., 2011. Homogeneous detection of concanavalin A using pyrene-conjugated maltose assembled graphene based on fluorescence resonance energy transfer. Biosens. Bioelectron. 26, 4497–4502.

Chen, D., Zhang, H., Liu, Y., Li, J.H., 2013. Graphene and its derivatives for the development of solar cells, photoelectrochemical, and photocatalytic applications. Energy Environ. Sci. 6, 1362–1387.

Cheng, C., Li, S., Zhao, J., Li, X., Liu, Z., Ma, L., Zhang, X., Sun, S., Zhao, C., 2013. Biomimetic assembly of polydopamine-layer on graphene: mechanisms, Versatile 2D and 3D architectures and pollutant disposal. Chem. Eng. J. 228, 468–481.

Chu, W., Rao, Y., Hui, W.Y., 2009. Removal of simazine in a UV/TiO_2 heterogeneous system. J. Agric. Food Chem. 57, 6944–6949.

Clemente, Z., Grillo, R., Jonsson, M., Santos, N.Z., Feitosa, L.O., Lima, R., Fraceto, L.F., 2014. Ecotoxicological evaluation of poly(epsilon-caprolactone) nanocapsules containing triazine herbicides. J. Nanosci. Nanotechnol. 7, 4911–4917.

Das, M.R., Sarma, R.K., Saikia, R., Kale, V.S., Shelke, M.V., Sengupta, P., 2011. Synthesis of silver nanoparticles in an aqueous suspension of graphene oxide sheets and its antimicrobial activity. Colloids Surf., B 83, 16–22.

Das, P., Borthakur, P., Boruah, P.K., Das, M.R., 2019. Peroxidase mimic activity of Au–Ag/L-Cys-rGO nanozyme toward detection of Cr(VI) ion in water: role of 3,3′,5,5′- tetramethylbenzidine adsorption. J. Chem. Eng. Data 64, 4977–4990.

Devipriya, S., Yesodharan, S., 2005. Photocatalytic degradation of pesticide contaminants in water. Sol. Energy Mater. Sol. Cells 86, 309–348.

Dong, X., Shi, Y., Zhao, Y., Chen, D., Ye, J., Yao, Y., Gao, F., Ni, Z., Yu, T., Shen, Z., Huang, Y., Chen, P., Li, L.J., 2009. Symmetry breaking of graphene monolayers by molecular decoration. J. Phys. Rev. Lett. 102, 135501.

Dong, Z., Wang, D., Liu, X., Pei, X., Chena, L., Jin, J., 2014. Bio-inspired surface-functionalization of graphene oxide for the adsorption of organic dyes and heavy metal ions with a superhigh capacity. J. Mater. Chem. 2, 5034–5040.

Gao, L.Z., Zhuang, J., Nie, L., Zhang, J.B., Zhang, Y., Gu, N., Wang, T.H., Feng, J., Yang, D.L., Perrett, S., Yan, X.Y., 2007. Intrinsic peroxidase-like activity of ferromagnetic nanoparticles. Nat. Nanotechnol. 2, 577–583.

Garg, B., Bisht, T., 2016. Carbon nanodots as peroxidase nanozymesfor biosensing. Molecules 21, 1653.

Ghandoor, H.E., Zidan, H.M., Khalil, M.I.M., 2012. Synthesis and some Physical properties of magnetite (Fe_3O_4) nanoparticles. Int. J. Electrochem. Sci. 7, 5734–5745.

Graziano, N., Mcguire, M.J., Roberson, A., Adams, C., Jiang, H., Blute, N., 2006. National atrazine occurrence monitoring program using the Abraxis ELISA method. Environ. Sci. Technol. 40, 1163–1171.

Han, X., Zhang, L., Li, C., 2014. Preparation of polydopamine-functionalized graphene–Fe3O4 magnetic composites with high adsorption capacities. RSC Adv. 4, 30536–30541.

Hosseini, M., Sabet, F.S., Khabbaz, H., Aghazadeh, M., 2017. Farhang mizanic and mohammad reza ganjali, enhancement of the peroxidase-like activity of cerium-doped ferrite nanoparticles for colorimetric detection of H_2O_2 and glucose. Anal. Methods 9, 3519–3524.

Huang, S.B., Mayer, T.J., Yokley, R.A., Perez, R., Agric, J., 2006. Direct aqueous injection liquid chromatography/electrospray ionization-mass spectrometry/mass spectrometry analysis of water for atrazine, simazine, and their chlorotriazine metabolites. J. Agric. Food Chem. 54, 713–719.

Huang, Y., Ren, J., Qu, X., 2019. Nanozymes: classification, catalytic mechanisms, activity regulation, and applications. Chem. Rev. 119, 4357–4412.

Ivanova, M.N., Grayfer, E.D., Plotnikova, E.E., Kibis, L.S., Darabdhara, G., Boruah, P.K., Das, M.R., Fedorov, V.E., 2019. Pt-decorated boron nitride nanosheets as artificial nanozymes for detection of dopamine. ACS Appl. Mater. Interfaces 11, 22102–22112.

Kamat, P.V., 2010. Graphene-based nanoarchitectures. Anchoring semiconductor and metal nanoparticles on a two-dimensional carbon support. J. Phys. Chem. Lett. 1, 520–527.

Kaminska, I., Das, M.R., Coffinier, Y., Niedziolka-Jonsson, J., Sobczak, J., Woisel, P., Lyskawa, J., Opallo, M., Boukherroub, R., Szunerits, S., 2012. Reduction and functionalization of graphene oxide sheets using biomimetic dopamine derivatives in one step. ACS Appl. Mater. Interfaces 4, 1016–1020.

Kaur, J., Singh, K.V., Boro, R., Thampi, K.R., Raje, M., Var-shney, G.C., Suri, R.C., 2007. Immunochromatographic dipstick assay format using gold nanoparticles labeled protein– hapten conjugate for the detection of atrazine. Environ. Sci. Technol. 41, 5028–5036.

Laurent, S., Forge, D., Port, M., Roch, A., Robic, C., Vander Elst, L., Muller, R.N., 2008.

Magnetic iron oxide nanoparticles: synthesis, stabilization, vectorization, physicochemical characterizations, and biological applications. Chem. Rev. 108, 2064–2110.
Lee, H., Dellatore, S.M., Miller, W.M., Messersmith, P.B., 2007. Mussel-inspired surface chemistry for multifunctional coatings. Science 318, 426–430.
Lee, D.-W., Kim, T., Lee, M., 2011. An amphiphilic pyrene sheet for selective functionalization of graphene. Chem. Commun 47, 8259–8261.
Li, W., Shang, T., Yang, W., Yang, H., Lin, S., Jia, X., Cai, Q., Yang, X., 2016. Effectively exerting the reinforcement of dopamine reduced graphene oxide on epoxy-based composites via strengthened interfacial bonding. ACS Appl. Mater. Interfaces 8, 13037–13050.
Li, D., Wang, S., Wang, L., Zhang, H., Hu, J.A., 2019. Simple colorimetric probe based on anti-aggregation of AuNPs for rapid and sensitive detection of malathion in environmental samples. Anal. Bioanal. Chem. 411, 2645–2652.
Lin, Y., Geng, Z., Cai, H., Ma, L., Chen, J., Zeng, J., Pan, N., Wang, X., 2012. Ternary graphene–TiO_2–Fe_3O_4, nanocomposite as a recollectable photocatalyst with enhanced durability. Eur. J. Inorg. Chem. 4439–4444.
Lomeda, J.R., Doyle, C.D., Kosynki, D.V., Hwang, W.F., Tour, J.M., 2008. Diazonium functionalization of surfactant-wrapped chemically converted graphene sheets. J. Am. Chem. Soc. 130, 16201–16206.
Ma, J.-L., Yin, B., Wu, Xin, Ye, B.-C., 2017. Simple and cost-effective glucose detection based on carbon nanodots supported on silver nanoparticles. Anal. Chem. 2, 1323–1328.
Manea, F., Houillon, F.B., Pasquato, L., Scrimin, P., 2004. Nanozymes: gold-nanoparticle-based transphosphorylation catalysts. Angew. Chem. Int. Ed. 43, 6165–6169.
Metin, O., Aydogan, S., Meral, K., 2014. A new route for the synthesis of graphene Oxide–Fe_3O_4 (GO–Fe_3O_4) nanocomposites and their Schottky diode applications. J. Alloys Compd. 185, 681–688.
Mnif, W., Hassine, A.I.H., Bouaziz, A., Bartegi, A., Thomas, O., Roig, B., 2011. Effect of endocrine disruptor pesticides: a review. Int. J. Environ. Res. Publ. Health 8 (6), 2265–2303.
Mohamed, H.H., 2019. Rationally designed Fe_2O_3/GO/WO_3 Z-Scheme photocatalyst for enhanced solar light photocatalytic water remediation. J. Photochem. Photobiol., A 378, 74–84.
Muenchen, D.K., Martinazzo, J., de Cezaro, A.M., Rigo, A.A., Brezolin, A.N., Manzoli, A., Leite, F.L., Steffens, C., Steffens, J., 2016. Pesticide detection in soil using biosensors and nanobiosensors. Biointerface Res. Appl. Chem. 6, 1659–1675.
Ouyang, L., Zhu, L., Jiang, J., Tang, H., 2014. A surface-enhanced Raman scattering method for detection of trace glutathione on the basis of immobilized silver nanoparticles and crystal violet probe. Anal. Chim. Acta 816, 41–49.
Palaniappan, N., Cole, I.S., Kuznetsov, A.E., Balasubramanian, K., Justin Thomas, K.R., 2019. Experimental and computational studies of a graphene oxide barrier layer covalently functionalized with amino acids on Mg AZ13 alloy in salt medium. RSC Adv. 9, 32441–32447.
Panias, D., Taxiarchou, M., Paspaliaris, I., Kontopoulos, A., 1996. Dis-solution of iron oxides in aqueous oxalic acid solutions. Hydrometallurgy 42, 257–265.
Polshettiwar, V., Luque, R., Fihri, A., Zhu, H., Bouhrara, M., Basset, J.M., 2011. Magnetically recoverable nanocatalysts. Chem. Rev. 111, 3036–3075.
Qiao, F., Wang, Z., Xu, K., Ai, S., 2015. Double enzymatic cascade reactions within FeSe–Pt@SiO_2 nanospheres: synthesis and application toward colorimetric biosensing of H_2O_2 and glucose. Analyst 140, 6684–6691.
R Rao, C.N., R, C.N., Sood, A.K., Subrahmanyam, K.S., Govindaraj, A., 2009. Graphene: the new two-dimensional nanomaterial. Angew. Chem. Int. Ed. 48, 7752–7777.
Rao, Y.F., Chu, W., 2013. Visible light-induced photodegradation of simazine in aqueous TiO_2 suspension. Ind. Eng. Chem. Res. 52, 13580–13586.
Segura, M.E.C., Gomez-Arroyo, S., Molina-Alvarez, B., Villalobos-Pietrini, R., Ezquerro, C.C., Cortes-Eslava, J., Valencia-Quintana, P.R., Lopez-Gonzalez, L., Zuniga-Reyes, R., Sanchez-Rincon, J., 2007. Metabolic activation of herbicide products by Vicia faba detected in human peripheral lymphocytes using alkaline single cell gel electrophoresis. Toxicol. Vitro 21, 1143–1154.
Sekhon, B., 2014. Nanotechnology in agri-food production: an overview. Nanotechnol. Sci. Appl. 7, 31–53.
Sheng, H., Li, Q., Ma, W., Ji, H., Chen, C., Zhao, J., 2013. Photocatalytic degradation of organic pollutants on surface anionized TiO_2: common effect of anions for high hole-availability by water. Appl. Catal., B 138, 212–218.
Shim, W.B., Yang, Z.Y., Kim, J.Y., Choi, J.G., Je, J.H., Kang, S.J., Kolosova, A.Y., Eremin, S.A., Chung, D.H., 2006. Immunochromatography using the colloidal gold-antibody probe for the detection of atrazine in water samples. J. Agric. Food Chem. 54, 9728–9734.
Srivastava, B., Jhelum, V., Basu, D.D., Patanjali, P.K., 2009. Adsorbents for pesticide uptake from contaminated water: a review. J. Sci. Ind. Res 68, 839–850.
Suhaimy, S.H.M., Hamid, S.B.A., Lai, C.W., Hasan, M.R., Johan, M.R., 2016. TiO_2 nanotubes supported Cu nanoparticles for improving photocatalytic degradation of simazine under UV illumination. Catalysts 6, 167.
Suhaimy, S.H.M., Lai, C.W., Tajuddin, H.A., Samsudin, E.M., Johan, M.R., 2018. Impact of TiO_2 nanotubes' morphology on the photocatalytic degradation of simazine. Pollutant, Materials 11, 2066.
Sun, Z., Zheng, S., Syoko, G.A., Frost, R.L., Xi, Y., 2013. Degradation of simazine from aqueous solutions by diatomite-supported nanosized zero-valent iron composite materials. J. Hazard Mater. 263, 768–777.
Varhese, N., Ghosh, A., Voggu, R., Gosh, S., Rao, C.N.R., 2009. Selectivity in the interaction of electron donor and acceptor molecules with graphene and single-walled carbon nanotubes. J. Phys. Chem. C 113, 16855–16859.
Wang, D., Astruc, D., 2014. Fast-Growing field of magnetically recyclable nanocatalysts. Chem. Rev. 114, 6949–6985.
Wang, H.-X., Zhou, K.-G., Xie, Y.-L., Zeng, J., Chai, N.-N., Li, J., Zhang, H.-L., 2011. Photoactive graphene sheets prepared by "click" chemistry. Chem. Commun. 47, 5747–5749.
Wei, H., Wang, E., 2013. Nanomaterials with enzyme-like characteristics (nanozymes): next-generation artificial enzymes. Chem. Soc. Rev. 42, 6060–6093.
Weng, B., Qi, M., Han, C., Tang, Z., Xu, Y., 2019. Photocorrosion inhibition of semiconductor-Based photocatalysts: basic principle, current development, and future perspec. ACS Catal. 9, 4642–4687.
Wu, Z., Tao, C., Lin, C., Shen, D., Li, G., 2008. Label-Free Colorimetric detection of trace atrazine in aqueous solution by using molecularly imprinted photonic polymers. Chem. Eur J. 14, 11358–11368.
Wu, Q., Zhao, J., Qin, G., Wang, C., Tong, X., Xue, S., 2013. Photocatalytic reduction of Cr(VI) with TiO_2 film under visible light. Appl. Catal., B 142, 142–148.
Wu, J., Wang, X., Wang, Q., Lou, X., Li, S., Zhou, Y., 2019. Nanomaterials with enzyme-like characteristics (nanoenzymes) : next generation artificial enzymes (II). Chem. Soc. Rev. 48, 1004–1076.
Xu, L.Q., Yang, W.J., Neoh, K.G., Kang, E.T., Fu, G.D., 2010. Dopamine-induced reduction and functionalization of graphene oxide nanosheets. Macromolecules 43, 8336–8339.
Xu, L.Q., Yang, W.J., Neoh, K.G., Kang, E.T., Fu, G.D., 2010. Dopamine-Induced reduction and functionalization of graphene oxide nanosheets. Macromolecules 43, 8336–8339.
Yang, L.P., Kong, J.H., Yee, W.A., Liu, W.S., Phua, S.L., Toh, C.L., Huang, S., Lu, X.H., 2012. Highly conductive graphene by low-temperature thermal reduction and in situ preparation of conductive polymer nanocomposites. Nanoscale 4, 4968–4971.